

Energy-dependent partial-wave analysis of all antiproton-proton scattering data below 925 MeV/ c

Daren Zhou¹ and Rob G. E. Timmermans¹

¹*KVI, Theory Group, University of Groningen,
Zernikelaan 25, NL-9747 AA Groningen, The Netherlands*

(Dated: September 19, 2021)

Abstract

We present a new energy-dependent partial-wave analysis of all antiproton-proton elastic ($\bar{p}p \rightarrow \bar{p}p$) and charge-exchange ($\bar{p}p \rightarrow \bar{n}n$) scattering data below 925 MeV/ c antiproton laboratory momentum. The long-range parts of the chiral one- and two-pion exchange interactions are included exactly. The short-range interactions, including the coupling to the mesonic annihilation channels, are parametrized by a complex boundary condition at a radius of $r = 1.2$ fm. The updated database, which includes significantly more high-quality charge-exchange data, contains 3749 scattering data. The fit results in $\chi^2_{\min}/N_{\text{df}} = 1.048$, where $N_{\text{df}} = 3578$ is the number of degrees of freedom. We discuss the description of the experimental data and we present the antiproton-proton phase-shift parameters.

PACS numbers: 13.75.Cs, 11.80.Et, 12.39.Fe, 21.30.Cb

I. INTRODUCTION

The antinucleon-nucleon ($\bar{N}N$) interaction at low energies is of fundamental interest, but progress towards understanding it has always been hindered by the lack of scattering data. Major steps forward were taken at the Low Energy Antiproton Ring (LEAR) at CERN in the 1980's and the early 1990's. For the first time, good-quality data became available for the total cross section and the total annihilation cross section as function of antiproton laboratory momentum (p_{lab}), for the analyzing power in antiproton-proton elastic scattering ($\bar{p}p \rightarrow \bar{p}p$), and for the differential cross section and analyzing power in charge-exchange scattering ($\bar{p}p \rightarrow \bar{n}n$), at antiproton momenta above about 200 MeV/ c . Unfortunately, LEAR was closed in 1996 and $\bar{p}p$ scattering experiments came to a halt. However, the enormous physics potential of a low-energy antiproton beam is clear, especially when it can be polarized, and in recent years the interest to investigate $\bar{p}p$ scattering has been revived, for instance by the collaboration for Polarized Antiproton eXperiments (PAX) [1].

The dominant feature of antiproton-proton scattering at low energy is the annihilation into mesons, a complex multiparticle process that is difficult to model. In pre-LEAR days, some qualitative understanding was obtained by using simplified prescriptions, such as a simple absorptive boundary condition [2–4] or a state-independent two- or three-parameter optical potential [5–12]. These models could describe the integrated total, annihilation, and charge-exchange cross sections, but not the differential observables. Motivated by the experiments at LEAR, more sophisticated $\bar{N}N$ models were developed in order to attempt a more quantitative fit to the data. Examples are the Paris optical-potential model [13–18] and the Nijmegen [19, 20] and Pittsburgh [21] coupled-channels models.

In Refs. [22–24] an energy-dependent partial-wave analysis (PWA) of all $\bar{p}p$ scattering data below $p_{\text{lab}} = 925$ MeV/ c was developed, in order to arrive at a model-independent description of the $\bar{N}N$ interaction. The method of analysis was adapted from the Nijmegen PWAs of the pp and np scattering data [25–29]. These PWAs exploit as much as possible our knowledge about the interaction in the description of the energy dependence of the scattering amplitudes. The long-range interactions, which are responsible for the rapid energy variations of the amplitudes, are included exactly in the Schrödinger equation, while the slow energy variations due to the essentially unknown short-range interactions are parametrized phenomenologically by a state- and energy-dependent boundary condition at some radius

$r = b$. In this way, an economic and model-independent high-quality description of the scattering database is possible. In the \overline{NN} case [22–24], one assumes that the long-range potential is given by the charge-conjugated version of a corresponding nucleon-nucleon (NN) potential, and, by implementing a complex boundary condition, one bypasses with this strategy as well our lack of knowledge of the short-range annihilation dynamics.

There are two important reasons to update the $\overline{p}p$ PWA of Ref. [23]. The first and perhaps main motivation is the renewed experimental interest in \overline{NN} scattering. The second reason is theoretical and is motivated by the progress reached in the last two decades in the understanding of the NN interaction within the framework of chiral effective field theory. In particular, the pp and np PWAs have been updated by including, next to the electromagnetic and the one-pion exchange (OPE) potential, the long-range parts of the chiral two-pion exchange (TPE) potential [28, 29], instead of the heavy-boson exchanges of the Nijmegen potential [30, 31], thereby improving even more the model independence and the quality of the NN PWAs of Refs. [25–27]. Motivated by that success, we include here as well the charge-conjugated TPE potential in the long-range \overline{NN} interaction, instead of the charge-conjugated heavy-boson exchanges that were used in Ref. [23].

At the same time, we take the opportunity to update the database of $\overline{p}p$ scattering data. The database constructed in Ref. [23] included all scattering data published in a regular physics journal up to early 1993. A number of high-quality data sets from LEAR became available only later, in particular differential cross sections and analyzing powers for the charge-exchange reaction $\overline{p}p \rightarrow \overline{n}n$. Also the first measurements of the depolarization and spin-transfer observables for $\overline{p}p \rightarrow \overline{n}n$ were published only later. These data sets can be included now and they provide significant new constraints on the PWA solution.

The organization of our paper is as follows: In Sec. II the method of PWA developed in Ref. [23] is reviewed. We summarize only the main points in order to make this paper self-contained and we emphasize the differences of our PWA with Ref. [23]. In Sec. III we discuss the boundary condition that parametrizes the short-range interaction. In Sec. IV the long-range \overline{NN} potential is discussed, in particular its chiral TPE component. In Sec. V, the new database is discussed and the statistical methods are reviewed. In Sec. VI we present the results of the PWA and discuss the description of the measured observables. In Sec. VII we present the \overline{NN} S matrix and phase-shift parameters. We conclude in Sec. VIII. An Appendix is devoted to a study of the statistical quality of the database.

II. THE METHOD OF ANALYSIS

For states with total angular momentum J , the radial part of the wave function for the antiproton-proton system, $\Phi^J(r)$, is obtained by solving the coupled-channels radial Schrödinger equation

$$\left[\frac{d^2}{dr^2} - \frac{L^2}{r^2} + p^2 - 2mV^J \right] \Phi^J(r) = 0 , \quad (1)$$

which is a differential equation in channel space. We include the channels $\bar{p}p$ and $\bar{n}n$. It is important to use this physical basis instead of the isospin basis, in order to be able to include the long-range electromagnetic interactions and to treat the threshold for charge-exchange scattering $\bar{p}p \rightarrow \bar{n}n$ at $p_{\text{lab}} \simeq 99 \text{ MeV}/c$ (or $T_{\text{lab}} \simeq 5.2 \text{ MeV}$) properly, which gives a much better description of the low-energy charge-exchange data. In Eq. (1), p is a diagonal matrix with the channel momenta p_a in the center-of-mass system, m is a diagonal matrix with the reduced mass m_a of the two scattered particles in channel a (so $m_a = M_p/2$ or $M_n/2$), and V^J is the potential with matrix elements $\langle \ell' s' a' | V^J(r) | \ell s a \rangle$. For partial waves with $\ell = J$, $s = 0, 1$, or $\ell = 1, J = 0$, the matrices are 2×2 , and for partial waves with $\ell = J \pm 1$ ($J \geq 1$), $s = 1$, coupled by the tensor force, the matrices are 4×4 . The relation between the total energy \sqrt{s} in the center-of-mass system and the channel momentum is given by the relativistic expression $\frac{1}{4}s = p_a^2 + 4m_a^2$.

We solve Eq. (1) numerically, starting with the boundary condition at $r = b$, up to “ $r = \infty$,” which in practice is a point outside of the range of the strong interaction. The asymptotic form of $\Phi^J(r)$ for $r = \infty$ can be written as

$$\Phi_{\text{as}}^J(r) \xrightarrow{r \rightarrow \infty} \sqrt{\frac{m}{p}} [H_1(pr)S^J + H_2(pr)] , \quad (2)$$

where S^J is the partial-wave S matrix and H_1 and H_2 are diagonal matrices. For the $\bar{p}p$ channel, where the Coulomb force acts, the entries are given by

$$\begin{aligned} H_\ell^{(1)}(\eta, pr) &= F_\ell(\eta, pr) - iG_\ell(\eta, pr) , \\ H_\ell^{(2)}(\eta, pr) &= F_\ell(\eta, pr) + iG_\ell(\eta, pr) , \end{aligned} \quad (3)$$

where F_ℓ and G_ℓ are the standard regular and irregular Coulomb wave functions; $\eta = \alpha/v_{\text{lab}}$ is the relativistic Coulomb parameter, where α is the fine-structure constant and v_{lab} is the velocity of the incoming antiproton in the laboratory frame. The asymptotic behavior of F_ℓ

and G_ℓ is

$$\begin{aligned} F_\ell(\eta, pr) &\stackrel{r \rightarrow \infty}{\sim} \sin \left[pr - \ell \frac{\pi}{2} + \sigma_\ell - \eta \ln(2pr) \right] , \\ G_\ell(\eta, pr) &\stackrel{r \rightarrow \infty}{\sim} \cos \left[pr - \ell \frac{\pi}{2} + \sigma_\ell - \eta \ln(2pr) \right] , \end{aligned} \quad (4)$$

where the Coulomb phase shift is $\sigma_\ell = \arg \Gamma(\ell + 1 + i\eta)$. For the $\bar{n}n$ channel, $\eta = 0$, and

$$F_\ell(0, \rho) = \rho j_\ell(\rho) , \quad G_\ell(0, \rho) = -\rho n_\ell(\rho) , \quad (5)$$

where $j_\ell(\rho)$ and $n_\ell(\rho)$ are the spherical Bessel and Neumann functions. The S matrix is obtained from the matching condition

$$W(\Phi^J(r_\infty), \Phi_{\text{as}}^J(r_\infty)) \equiv 0 , \quad (6)$$

where Φ^J is the numerical solution of Eq. (1) and Φ_{as}^J is given by Eq. (2). The Wronskian is defined by

$$W(\Phi_1, \Phi_2) = \Phi_1^T \frac{1}{m} \Phi_2' - \Phi_1'^T \frac{1}{m} \Phi_2 , \quad (7)$$

where the prime denotes differentiation with respect to r and “T” means transposition. This gives for the partial-wave S matrix

$$S^J = - \left[(\Phi^J)'^T \frac{1}{\sqrt{mp}} H_1 - (\Phi^J)^T \sqrt{\frac{p}{m}} H_1' \right]^{-1} \left[(\Phi^J)'^T \frac{1}{\sqrt{mp}} H_2 - (\Phi^J)^T \sqrt{\frac{p}{m}} H_2' \right] ; \quad (8)$$

the prime on the Hankel functions denotes differentiation with respect to the argument pr .

Due to the presence of the long-range electromagnetic interaction, care has to be taken to define the S matrix (*i.e.* the phase-shift parameters) [23, 25, 32]. We include in the potential the long-range parts of the Coulomb, the magnetic-moment, and the strong (one- and two-pion exchange) interactions, $V = V_C + V_{MM} + V_N$. We integrate the Schrödinger equation up to a point outside the range of the strong interaction, where we match to Coulomb (for $\bar{p}p$) and Bessel (for $\bar{n}n$) wave functions. The S matrix is therefore defined with respect to the Coulomb force that acts in the $\bar{p}p$ channel. Because we need to include the infinite-range Coulomb interaction and part of the magnetic-moment interaction in all partial waves, but the finite-range nuclear interaction only up to some maximum value of J , we decompose the S matrix in order to split off the Coulomb part and the magnetic-moment part as

$$\begin{aligned} S_{C+MM+N} - 1 &= (S_C - 1) + S_C^{1/2} (S_{C+MM}^C - 1) S_C^{1/2} + \\ &\quad S_C^{1/2} (S_{C+MM}^C)^{1/2} (S_{C+MM+N}^{C+MM} - 1) (S_{C+MM}^C)^{1/2} S_C^{1/2} , \end{aligned} \quad (9)$$

where S_C is the Coulomb S matrix with matrix elements $\langle \ell' s' | S_C | \ell s \rangle = \delta_{\ell\ell'} \delta_{ss'} \exp(2i\sigma_\ell)$ in the $\bar{p}p$ channel and zero in the $\bar{n}n$ channel. In Eq. (9) we used matrix notation, because the magnetic-moment interaction contains a tensor part and the S matrix is not diagonal in orbital angular momentum; its square root is well-defined, however.

The scattering amplitude is correspondingly decomposed as

$$M_{C+MM+N}(\theta) = M_C(\theta) + M_{C+MM}^C(\theta) + M_{C+MM+N}^{C+MM}(\theta), \quad (10)$$

where $M_C(\theta)$ is the Coulomb scattering amplitude, $M_{C+MM}^C(\theta)$ is the magnetic-moment scattering amplitude in the presence of the Coulomb interaction, and $M_{C+MM+N}^{C+MM}(\theta)$ is the scattering amplitude for the strong interaction in the presence of the Coulomb and magnetic-moment interactions. The matrix elements of $M_C(\theta)$ for $\bar{p}p$ scattering are given by

$$\begin{aligned} \langle s' m' | M_C(\theta) | s m \rangle &= -\delta_{ss'} \delta_{mm'} \frac{\eta}{p(1 - \cos \theta)} e^{-i\eta \ln \frac{1}{2}(1 - \cos \theta) + 2i\sigma_0} \\ &= -\delta_{ss'} \delta_{mm'} \frac{\eta}{2p} \frac{e^{2i\sigma_0}}{(\sin^2 \frac{1}{2}\theta)^{1+i\eta}}. \end{aligned} \quad (11)$$

The matrix elements $M_{C+MM}^C(\theta)$ of the magnetic-moment interaction are calculated in Coulomb distorted-wave Born approximation [23, 32]. The partial-wave decomposition of the nuclear scattering amplitude is given by

$$\begin{aligned} \langle s' m' a' | M_{C+MM+N}^{C+MM}(\theta) | s m a \rangle &= \sum_{\ell \ell' J} \sqrt{4\pi(2\ell+1)} i^{\ell-\ell'} C_{0 m m}^{\ell s J} C_{m-m' m' m}^{\ell' s' J} Y_{m-m'}^{\ell'}(\theta) \\ &\quad \langle \ell' s' a' | S_C^{1/2} (S_{C+MM}^C)^{1/2} (S_{C+MM+N}^{C+MM} - 1) (S_{C+MM}^C)^{1/2} S_C^{1/2} | \ell s a \rangle / 2ip_a, \end{aligned} \quad (12)$$

where a denotes the channel $\bar{p}p$ or $\bar{n}n$. Because S_{C+MM+N}^{C+MM} is difficult to calculate it is approximated by $S_{C+MM+N}^{C+MM} \simeq S_{C+N}^C$, where S_{C+N}^C is the S matrix for the strong interaction in the presence of the Coulomb interaction. From the scattering amplitude on the spin-singlet, spin-triplet basis, all the observables can be calculated [33].

III. THE BOUNDARY CONDITION APPROACH

The coupled-channels Schrödinger equation, Eq. (1), is solved with a boundary condition at a radius $r = b$, for each energy and for each partial wave. The fit to the data is not very sensitive to the exact value of b , but in our case an optimal value $b = 1.2$ fm was found. For the specific form of the partial-wave boundary condition we define the P matrix [34, 35] by

$$P^J = b \left[(\Phi^J)^{-1} \left(\frac{d\Phi^J}{dr} \right) \right]_{r=b}, \quad (13)$$

where $\Phi^J(r)$ is the radial wave function. The P matrix parametrizes the complicated short-range interaction of the $\bar{p}p$ system. The coupling of the $\bar{p}p$ and $\bar{n}n$ channels to the mesonic annihilation channels is taken into account by a complex P matrix.

The P matrix is a powerful tool in a PWA, since it provides the separation between the long-range interaction, which is relatively model independent and taken into account exactly in the Schrödinger equation, and the short-range interaction, which is essentially unknown and parametrized completely phenomenologically. The long-range interactions cause the rapid energy dependence of the scattering amplitudes, while the short-range interactions result in slow energy variations. The results, for that reason, do not depend on the details of the short-range interactions. We therefore choose a simple parametrization for the P matrix, which corresponds to a state-dependent, *i.e.* spin- and isospin-dependent, short-range optical potential. We assume that the interaction in each partial wave can be parametrized by a complex spherical well, the depth of which is different for elastic and charge-exchange scattering, *i.e.* for $I = 0$ and $I = 1$. For a single-channel partial wave with orbital angular momentum ℓ , isospin I , and with the spherical well $V_I + iW_I$, the P matrix is given by

$$P_\ell = p'b J'_\ell(p'b)/J_\ell(p'b) , \quad (14)$$

where $J_\ell(\rho) = \rho j_\ell(\rho)$ and $p'^2 = p^2 - \overline{M}(V_I + iW_I)$, where $\overline{M} = (M_p + M_n)/2$.

The P matrix is calculated on the isospin basis and then transformed to the physical particle basis with the channels $\bar{p}p$, $\bar{n}n$. For the uncoupled partial waves with $\ell = J$, $s = 0, 1$, or $\ell = 1$, $J = 0$, it is therefore a 2×2 matrix. For the partial waves with $\ell = J \pm 1$ ($J \geq 1$), $s = 1$, coupled by the tensor force, we introduce for each value of the isospin I an additional mixing angle θ_{IJ} between the partial waves with $\ell = J - 1$ and $\ell = J + 1$. We write

$$P^J = \begin{pmatrix} \cos \theta_{IJ} & \sin \theta_{IJ} \\ -\sin \theta_{IJ} & \cos \theta_{IJ} \end{pmatrix} \begin{pmatrix} P_{J-1} & 0 \\ 0 & P_{J+1} \end{pmatrix} \begin{pmatrix} \cos \theta_{IJ} & -\sin \theta_{IJ} \\ \sin \theta_{IJ} & \cos \theta_{IJ} \end{pmatrix} , \quad (15)$$

where P_{J-1} and P_{J+1} are the single-channel P matrices of Eq. (14) for $\ell = J - 1$ and $\ell = J + 1$, respectively. On the particle basis, the P matrix for these coupled states is 4×4 .

In Ref. [23], the imaginary parts of the square wells were assumed to be equal for $I = 0$ and $I = 1$ in each partial wave. We take these to be different here, because this choice gives a better fit to the more recent high-quality charge-exchange data. The fitted values of the P -matrix parameters are given in Table I. The fit to 3749 scattering data requires a total of 46

TABLE I. P -matrix parameters for the different partial waves. V_0 and V_1 are the real parts and W_0 and W_1 are the imaginary parts of the short-range spherical-well potential, for isospin $I = 0$ and $I = 1$, respectively. The values of the mixing angles θ_{IJ} that parametrize the off-diagonal P matrix for the partial waves coupled by the tensor force are: $\theta_{01} = 7.6^\circ \pm 0.4^\circ$ and $\theta_{11} = -10.7^\circ \pm 0.8^\circ$ for the 3S_1 - 3D_1 waves; $\theta_{02} = 0.0^\circ$ and $\theta_{12} = -8.8^\circ \pm 1.6^\circ$ for the 3P_2 - 3F_2 waves; $\theta_{03} = -7.4^\circ \pm 0.4^\circ$ and $\theta_{13} = -6.9^\circ \pm 1.4^\circ$ for the 3D_3 - 3G_3 waves. The quoted errors are defined as the change in each parameter that gives a rise in χ^2_{\min} of 1 when the remaining parameters are refitted.

Partial wave	V_0 (MeV)	W_0 (MeV)	V_1 (MeV)	W_1 (MeV)
1S_0	0	-161.7(25.2)	-516.1(19.4)	-132.8(19.9)
3S_1	-135.6(9.5)	-166.9(8.3)	33.6(5.7)	-166.3(8.0)
1P_1	0	-374.5(29.6)	0	-413.8(40.7)
3P_0	-114.9(10.1)	-142.8(9.3)	-164.1(4.5)	-71.9(6.9)
3P_1	-78.0(4.2)	-62.2(3.7)	0	-382.2(27.6)
3P_2	-114.6(5.7)	-201.4(5.1)	-41.4(3.0)	-135.6(5.4)
1D_2	-277.8(16.2)	-330.8(27.0)	-319.6(30.4)	-482.8(45.8)
3D_1	0	-96.6(15.5)	0	-129.4(19.7)
3D_2	-120.7(17.6)	-95.5(16.8)	0	-338.6(27.3)
3D_3	-235.7(7.7)	-181.1(8.4)	-102.0(9.1)	-66.6(7.8)
1F_3	-510.0(22.9)	-312.4(35.6)	0	-335.3(82.0)
3F_2	0	-356.0(56.6)	-554.0(26.5)	-317.1(27.0)
3F_4	-498.4(61.0)	-423.2(46.6)	0	0

P -matrix parameters. Almost all the short-range square-well potentials are attractive. The quoted errors reflect the sensitivity of the fit to variations in the corresponding parameters. These errors are defined as the change in each parameter that gives a rise in χ^2_{\min} of 1 when the remaining parameters are refitted. The lower partial waves all require parameters to obtain a good fit. To decide which parameters to keep in the fit, a three-sigma criterion is used: When the error turns out to be more than one third of the parameter value, it implies that χ^2_{\min} rises by less than 9 when the remaining parameters are refitted. In that case the parameter is set to zero, *i.e.* it is left out. Because of the centrifugal barrier, the fit becomes progressively less sensitive to short-range parameters for the higher- ℓ partial waves. We

assume the parameters in these partial waves to be equal to the ones in similar lower partial waves. For example, the parameters for the 3F_3 and 3G_4 waves are taken to be the same as the ones for 3D_2 ; the ones for 1G_4 and 1H_5 are the same as the ones for 1F_3 ; and the ones for 3G_5 and 3H_6 are the same as the ones for 3F_4 . We include the partial waves as high as $J = 12$, which is for instance needed to describe the forward “spike” in the charge-exchange differential cross section.

IV. THE LONG-RANGE ANTINUCLEON-NUCLEON POTENTIAL

The potential tail for $r > b$ includes the electromagnetic and the strong (nuclear) interaction V_N , where the electromagnetic interaction is the one-photon exchange potential, *i.e.* the Coulomb potential and the magnetic-moment interaction [32],

$$V = V_C + V_{MM} + V_N . \quad (16)$$

In contrast to the NN PWAs, we do not include the vacuum-polarization potential, because its effects are negligible, except for very low energies [25], where there are no $\bar{p}p$ scattering data available. Two-photon exchange effects [36] are not taken into account either.

The Coulomb potential acts only in the $\bar{p}p$ channel and is given by the expression

$$V_C(r) = -\frac{\alpha'}{r} , \quad (17)$$

where α' takes care of the main relativistic corrections to the Coulomb potential. It is defined by the relativistic Coulomb factor $\eta = \alpha' M_p / (2p)$. The magnetic-moment potential in the $\bar{p}p$ channel is given by

$$V_{MM}(r) = \frac{\mu_p^2}{4M_p^2} \frac{\alpha}{r^3} S_{12} + \frac{8\mu_p - 2}{4M_p^2} \frac{\alpha}{r^3} \mathbf{L} \cdot \mathbf{S} , \quad (18)$$

where $\mu_p = 1 + \kappa_p = 2.793$, with κ_p the anomalous magnetic moment of the proton; the tensor operator $S_{12} = 3 \boldsymbol{\sigma}_1 \cdot \hat{\mathbf{r}} \boldsymbol{\sigma}_2 \cdot \hat{\mathbf{r}} - \boldsymbol{\sigma}_1 \cdot \boldsymbol{\sigma}_2$, with $\boldsymbol{\sigma}_1$ and $\boldsymbol{\sigma}_2$ the spin operators of the two nucleons, \mathbf{L} is the angular momentum vector, and $\mathbf{S} = (\boldsymbol{\sigma}_1 + \boldsymbol{\sigma}_2)/2$ the total spin. The spin-orbit potential is due to the interaction of the magnetic moment of one particle with the charge of the other particle and includes a relativistic correction from the Thomas precession. The tensor force is due to the interaction between the magnetic moments of the two particles. The magnetic-moment interaction in the $\bar{n}n$ channel contains only the tensor-force part of Eq. (18) with $\mu_n = \kappa_n = -1.913$ and M_n .

The nuclear potential V_N contains the OPE and TPE potentials for $\bar{N}N$ scattering. Since the strong interaction is invariant under charge conjugation C , the $\bar{N}N$ potential can be obtained from the NN potential by using the operator C . If one assumes that isospin symmetry $SU(2, I)$ is exact, one can also use the G -parity operator, which is defined as $G = C \exp(i\pi I_2)$, and thus contains charge conjugation and a rotation in isospin space. The OPE potential is isospin dependent, while the TPE potential contains both isospin-independent and isospin-dependent parts. When we define the nuclear potential in isospin space for the NN system by

$$V_N(NN) = W_\pi \vec{\tau}_1 \cdot \vec{\tau}_2 + V_{2\pi} + W_{2\pi} \vec{\tau}_1 \cdot \vec{\tau}_2 , \quad (19)$$

the potential for the $\bar{N}N$ system is given by

$$V_N(\bar{N}N) = -W_\pi \vec{\tau}_1 \cdot \vec{\tau}_2 + V_{2\pi} + W_{2\pi} \vec{\tau}_1 \cdot \vec{\tau}_2 , \quad (20)$$

which implies for elastic and charge-exchange scattering, respectively,

$$\begin{aligned} V_N(\bar{p}p \rightarrow \bar{p}p) &= W_\pi + V_{2\pi} - W_{2\pi} , \\ V_N(\bar{p}p \rightarrow \bar{n}n) &= 2 (W_\pi - W_{2\pi}) , \end{aligned} \quad (21)$$

where the factor 2 is due to isospin symmetry.

The TPE potential for NN scattering has been derived from the effective nonlinear chiral Lagrangian density, which implements the spontaneously broken $SU(2, L) \otimes SU(2, R)$ chiral symmetry of QCD [28, 37, 38]. The leading order of this effective Lagrangian density is the nonlinear Weinberg model,

$$\mathcal{L}^{(0)} = -\bar{N} \left[\gamma_\mu \mathcal{D}^\mu + M + ig_A \gamma_5 \gamma_\mu \vec{\tau} \cdot \vec{D}^\mu \right] N , \quad (22)$$

with the chiral-covariant derivative

$$\mathcal{D}^\mu N = \left(\partial^\mu + \frac{i}{F_\pi} c_0 \vec{\tau} \cdot \vec{\pi} \times \vec{D}^\mu \right) N , \quad (23)$$

where $\vec{D}^\mu = D^{-1} \partial^\mu \vec{\pi} / F_\pi$ and $D = 1 + \vec{\pi}^2 / F_\pi^2$; M is the mass of the nucleon, $g_A = 1.269$ is the Gamow-Teller coupling constant in neutron β decay, and $F_\pi = 185$ MeV is the pion decay constant. The subleading-order chiral Lagrangian density is

$$\mathcal{L}^{(1)} = -\bar{N} \left[8c_1 D^{-1} m_\pi^2 \vec{\pi}^2 / F_\pi^2 + 4c_3 \vec{D}_\mu \cdot \vec{D}^\mu + 2c_4 \sigma_{\mu\nu} \vec{\tau} \cdot \vec{D}^\mu \times \vec{D}^\nu \right] N . \quad (24)$$

The constant $c_0 = 1$ multiplying the Weinberg-Tomozawa $NN\pi\pi$ interaction is fixed by chiral symmetry. However, the coupling constants c_j ($j = 1, 3, 4$) are low-energy constants that have to be determined from experimental data. These constants are of order $\mathcal{O}(1/M)$ and their values contain contributions from the “integrated-out” heavy hadrons, in particular the N - and Δ -isobars, and the two-pion resonances $\varepsilon(760)$ and $\rho(770)$. (The constant c_2 does not contribute to NN scattering at this order.)

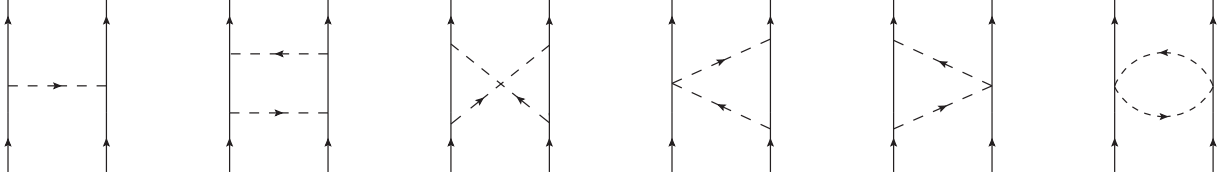


FIG. 1. The Feynman diagrams for one- and two-pion exchange.

The Feynman diagrams for the OPE and TPE processes are shown in Fig. 1, where the OPE diagram and the planar- and crossed-box TPE diagrams come from Eq. (22), the “triangle” and “football” TPE diagrams containing the Weinberg-Tomozawa $NN\pi\pi$ interaction also come from Eq. (22), while the other “triangle” TPE diagrams containing the c_j ($j = 1, 3, 4$) $NN\pi\pi$ interactions come from Eq. (24). The pion-exchange potentials of Eq. (19) contain isospin-independent and isospin-dependent central, spin-spin, tensor, and spin-orbit terms,

$$V_N = V_C + V_S \boldsymbol{\sigma}_1 \cdot \boldsymbol{\sigma}_2 + V_T S_{12} + V_{SO} \mathbf{L} \cdot \mathbf{S} \\ + (W_C + W_S \boldsymbol{\sigma}_1 \cdot \boldsymbol{\sigma}_2 + W_T S_{12} + W_{SO} \mathbf{L} \cdot \mathbf{S}) \vec{\tau}_1 \cdot \vec{\tau}_2, \quad (25)$$

where for OPE only the coefficients W_S and W_T are nonzero, and TPE contains in leading order only the terms V_S , V_T , and W_C , whereas in subleading order all the terms are nonzero. The coefficients in Eq. (25) are written in terms of dimensionless functions as

$$V_i(r) + W_i(r) \vec{\tau}_1 \cdot \vec{\tau}_2 = f^{2n} \xi^{2n} [v_i(x) + w_i(x) \vec{\tau}_1 \cdot \vec{\tau}_2] m_\pi, \quad (26)$$

with $n = 1$ for OPE and $n = 2$ for TPE, $i = C, S, T, SO$, and $x = m_\pi r$. We use the conventional rationalized “pseudovector” $NN\pi$ coupling constant f , normalized such that $f^2 \simeq 0.075$ [39, 40]. This means that we introduced the scaling mass m_s , chosen to be numerically equal to the charged-pion mass $m_s = m_{\pi^+}$, and we defined $\xi = m_\pi/m_s$. If the Goldberger-Treiman relation were exact, one would have that $g_A/F_\pi = \sqrt{4\pi}f/m_s$.

The OPE potential contains isospin-dependent spin-spin and tensor parts, with

$$\begin{aligned} w_S(x) &= e^{-x}/3x , \\ w_T(x) &= (1 + x + x^2/3) e^{-x}/x^3 . \end{aligned} \quad (27)$$

For the leading- and subleading-order TPE potential, the isospin-independent and the isospin-dependent parts can be written as

$$\begin{aligned} v_i(x) &= \frac{2}{\pi} v_{i,1}(x) + \frac{m_\pi}{M_p} v_{i,2}(x) , \\ w_i(x) &= \frac{2}{\pi} w_{i,1}(x) + \frac{m_\pi}{M_p} w_{i,2}(x) , \end{aligned} \quad (28)$$

where the subscript 1 indicates leading-order and the subscript 2 subleading order. The leading-order, static TPE potential contains isospin-independent spin-spin and tensor terms and an isospin-dependent central term, with

$$\begin{aligned} v_{S,1}(x) &= 12K_0(2x)/x^3 + (12 + 8x^2)K_1(2x)/x^4 , \\ v_{T,1}(x) &= -12K_0(2x)/x^3 - (15 + 4x^2)K_1(2x)/x^4 , \\ w_{C,1}(x) &= (\tilde{c}_0^2 + 10\tilde{c}_0 - 23 - 4x^2) K_0(2x)/x^3 \\ &\quad + [\tilde{c}_0^2 + 10\tilde{c}_0 - 23 + (4\tilde{c}_0 - 12)x^2] K_1(2x)/x^4 , \end{aligned} \quad (29)$$

where $\tilde{c}_0 = c_0/\tilde{g}_A^2$ with $\tilde{g}_A = F_\pi\sqrt{4\pi}f/m_s$ and $K_n(2x)$ ($n = 0, 1$) are the modified Bessel functions (the hyperbolic Bessel functions) of the second kind, which have asymptotic behavior $K_n(2x) \sim \sqrt{\pi/4x} e^{-2x}$ for $x \rightarrow \infty$. The subleading-order potential contains nonstatic terms from Eq. (22) and the leading-order terms from Eq. (24), which can be written as

$$v_{i,2}(x) = \sum_{k=1}^6 a_k e^{-2x}/x^k , \quad (30)$$

and similarly for the $w_{i,2}(x)$ terms. The coefficients a_k are listed in Table II, where we defined $\tilde{c}_j = c_j M_p/\tilde{g}_A^2$ ($j = 1, 3, 4$) and $\tilde{c}_{04} = \tilde{c}_0 + 4\tilde{c}_4$.

The OPE and TPE potentials for $\bar{p}p \rightarrow \bar{p}p$ and for $\bar{p}p \rightarrow \bar{n}n$ are now given by Eq. (21). In the OPE potential, we take m_π for $\bar{p}p$ and $\bar{n}n$ elastic scattering to be the neutral-pion mass m_{π^0} and for charge-exchange scattering the charged-pion mass m_{π^+} . In the PWAs of Refs. [22, 23], the pion-nucleon coupling constant $f_c^2 = f_{pn\pi^+}f_{np\pi^-}/2$ was determined from the charge-exchange data. In Ref. [22] $f_c^2 = 0.0751(17)$ was found, and in Ref. [23] $f_c^2 = 0.0732(11)$. The values were consistent with the values for $f_{pp\pi^0}^2$ and f_c^2 found in the

TABLE II. The coefficients of the subleading-order TPE potential of Eq. (30) for the central, spin-spin, tensor, and spin-orbit terms [28]; we define $\tilde{c}_0 = c_0/\tilde{g}_A^2$; $\tilde{c}_j = c_j M_p/\tilde{g}_A^2$ for $j = 1, 3, 4$, and $\tilde{c}_{04} = \tilde{c}_0 + 4\tilde{c}_4$.

	a_1	a_2	a_3	a_4	a_5	a_6
$v_{C,2}$	3/4	$9 + 48\tilde{c}_1 + 24\tilde{c}_3$	$27 + 96\tilde{c}_1 + 96\tilde{c}_3$	$99/2 + 48\tilde{c}_1 + 240\tilde{c}_3$	$54 + 288\tilde{c}_3$	$27 + 144\tilde{c}_3$
$v_{S,2}$		-3	-9	-33/2	-18	-9
$v_{T,2}$		3/2	27/4	15	18	9
$v_{SO,2}$			-12	-36	-48	-24
$w_{C,2}$	3/2	$4 - 2\tilde{c}_0$	$14 - 8\tilde{c}_0$	$31 - 20\tilde{c}_0$	$36 - 24\tilde{c}_0$	$18 - 12\tilde{c}_0$
$w_{S,2}$		-2/3	$-14/3 + 8\tilde{c}_{04}/3$	$-31/3 + 20\tilde{c}_{04}/3$	$-12 + 8\tilde{c}_{04}$	$-6 + 4\tilde{c}_{04}$
$w_{T,2}$		1/3	$17/6 - 4\tilde{c}_{04}/3$	$26/3 - 16\tilde{c}_{04}/3$	$12 - 8\tilde{c}_{04}$	$6 - 4\tilde{c}_{04}$
$w_{SO,2}$				$8 - 8\tilde{c}_0$	$16 - 16\tilde{c}_0$	$8 - 8\tilde{c}_0$

pp and np PWAs [39], resulting in the recommended value $f^2 = f_{NN\pi}^2 = 0.0750(9)$ for the pion-nucleon coupling constant, with no significant evidence for isospin breaking [40]. We have taken here the values $f_{pp\pi^0}^2 = 0.075$ and $f_c^2 = 0.075$ for the OPE potential for elastic and charge-exchange scattering, respectively. In the TPE potential we use for m_π the average pion mass $(2m_{\pi^+} + m_{\pi^0})/3 = 138.04$ MeV and the charge-independent coupling constant $f^2 = f_{NN\pi}^2 = 0.075$. The strong potentials for $\bar{n}n \rightarrow \bar{n}n$ and $\bar{n}n \rightarrow \bar{p}p$ are equal to the ones for $\bar{p}p \rightarrow \bar{p}p$ and $\bar{p}p \rightarrow \bar{n}n$, respectively.

The values of c_j ($j = 1, 3, 4$) were determined in the pp and np PWAs [28, 29]. The c_1 term in Eq. (24) breaks chiral symmetry explicitly, since it is proportional to m_π . The value of c_1 cannot be determined accurately from the NN data. It was fixed theoretically at $c_1 = -0.76/\text{GeV}$ by assuming a value for the pion-nucleon sigma term [28]. We take the same value here. It is interesting, however, to probe the sensitivity of our results to variations in c_3 and c_4 . It is difficult to determine c_3 and c_4 and their statistical errors by a fit to the database. Since they are parameters in the long-range interaction for $r > b$, this would require that for each small step in varying c_3 or c_4 , the Schrödinger equation would have to be solved for all the energies. However, we found that very good results were obtained for the values $c_3 = -5.8/\text{GeV}$ and $c_4 = 4.0/\text{GeV}$, where we estimate the uncertainties to be of the order of 0.5. This means that the values we found are remarkably

consistent with the values determined in the pp PWA to 350 MeV: $c_3 = -5.08(28)/\text{GeV}$ and $c_4 = 4.70(70)/\text{GeV}$ [28]. In the pp and np PWA to 500 MeV the values $c_3 = -4.78(10)/\text{GeV}$ and $c_4 = 3.96(22)/\text{GeV}$ were found [29]. One could interpret this as a demonstration of charge conjugation invariance of the TPE interaction. We leave a more careful study of the chiral OPE and TPE potential tail in \overline{NN} scattering for the future.

The resulting long-range OPE and TPE potentials should be compared to the ones of Ref. [23] where the charge-conjugated version of the high-quality soft-core Nijmegen one-boson exchange (OBE) potential [30, 31] was used as long-range interaction. In both cases, OPE is included, so one should compare TPE to the exchange of the heavy bosons, in particular the two-pion resonances $\varepsilon(760)$ and $\rho(770)$. Since the vector mesons have negative charge parity, the coupling constants of $\rho(770)$ and $\omega(782)$ change sign when going from nucleons to antinucleons. When we write schematically for the pp potential

$$V(pp \rightarrow pp) = W_\pi + V_\varepsilon + W_\rho + V_\omega + \dots, \quad (31)$$

we obtain for the OBE potential for elastic $\overline{p}p \rightarrow \overline{p}p$ and charge-exchange $\overline{p}p \rightarrow \overline{n}n$ scattering

$$\begin{aligned} V(\overline{p}p \rightarrow \overline{p}p) &= W_\pi + V_\varepsilon - W_\rho - V_\omega + \dots, \\ V(\overline{p}p \rightarrow \overline{n}n) &= 2(W_\pi - W_\rho + \dots), \end{aligned} \quad (32)$$

respectively. This should be compared to Eq. (21). It implies that for the NN case the central potential is relatively weak, because there is a cancellation between the repulsion due to the vector mesons and the attraction due to the scalar mesons, there is a strong coherent spin-orbit force from the exchange of the scalar and vector mesons, and the tensor forces due to OPE and $\rho(770)$ exchange have opposite sign. For the \overline{NN} case, a strong coherent central attraction results due to scalar- and vector-meson exchange and a relatively weak spin-orbit potential. Moreover, a strong coherent tensor potential acts in \overline{NN} due to OPE and $\rho(770)$ exchange. This strong tensor force dominates the charge-exchange $\overline{p}p \rightarrow \overline{n}n$ and strangeness-exchange $\overline{p}p \rightarrow \overline{\Lambda}\Lambda$ processes, where no neutral mesons can be exchanged [41–44].

The chiral TPE potential in subleading order has qualitatively a number of similar features. Because the values of c_3 and c_4 are large, the corresponding “triangle” diagrams with an $NN\pi\pi$ “seagull” interaction lead to relatively strong potentials. The c_3 term gives rise to a strong central attraction, while the c_4 term gives rise to a strong tensor force with the

same sign as the tensor force due to OPE. This results in a strong attractive central force in the elastic process $\bar{p}p \rightarrow \bar{p}p$ and a strong coherent tensor force in the charge-exchange process $\bar{p}p \rightarrow \bar{n}n$. This can be understood because the c_3 and c_4 terms contain effects from “integrated-out” $\varepsilon(760)$ scalar-isoscalar and $\rho(770)$ vector-isovector mesons, respectively. In fact, these two mesons are prominent broad two-pion resonances. In the potential of Refs. [30, 31] their widths are treated in a two-pole approximation; the lowest-mass poles correspond to mesons of masses of about 550 and 650 MeV, respectively, resulting in relatively long-range potentials.

V. ANTIPROTON-PROTON DATABASE AND STATISTICS

The antiproton-proton database was constructed for the first time in Ref. [23]. It included all available scattering data below antiproton laboratory momentum 925 MeV/ c published up to early 1993 in a regular physics journal, *i.e.* total and annihilation cross sections, differential cross sections and analyzing powers for elastic and charge-exchange scattering, total cross sections for charge-exchange scattering, and (very few) differential depolarizations for elastic scattering. At that time, most of the experiments at LEAR were finished. However, some more data sets were published after the completion of the PWA of Ref. [23]. We include these data sets here, along with a few data sets for which the numerical values were not available back then. The present, new database is summarized in Table III. The data sets that were not included in Ref. [23] are marked with an asterisk in the left column. We always consult the original publications for information about the data and their statistical and systematic uncertainties.

Statistical tools are an essential part of the data analysis in a PWA. We use exactly the same methods as in the NN PWAs [25]. We mention here only the main relevant points, more details can be found in Ref. [23]. We perform a least-squares fit of the model parameters to the total database, which contains individual data sets labelled by A . One data set contains N_A individual data points labelled by i . The χ^2 of the fit is correspondingly defined as

$$\chi^2(\mathbf{p}) = \sum_A \chi_A^2(\mathbf{p}) = \sum_A \min \left[\sum_{i=1}^{N_A} \left(\frac{M_{A,i}(\mathbf{p}) - \nu_A E_{A,i}}{\epsilon_{A,i}} \right)^2 + \left(\frac{\nu_A - 1}{\epsilon_{A,0}} \right)^2 \right], \quad (33)$$

where \mathbf{p} is the parameter vector with N_{par} entries, $M_{A,i}(\mathbf{p})$ is the value predicted by the model for the measured observable $E_{A,i}$ labelled i in set A with statistical error $\epsilon_{A,i}$ (in

several cases, point-to-point systematic errors were added in quadrature to the statistical errors in the experimental papers). In most cases, the data sets have an overall normalization uncertainty, denoted by $\epsilon_{A,0}$, specified by the experimentalists. For each of these sets we introduce a normalization parameter ν_A that multiplies the measured values $E_{A,i}$ of the entire set. In the case that the experimental data sets are only relative, or in the case that the normalization error was underestimated, the error $\epsilon_{A,0}$ is taken to be ∞ (in practice very large) and the corresponding normalization parameter ν_A is “floated.” The contributions to χ^2 of these normalizations are then zero. In a few cases the normalizations are absolute, *i.e.* $\epsilon_{A,0} = 0$, and the contributions to χ^2 of these normalizations are again zero.

By using a sophisticated numerical fitting code, the value of $\chi^2(\mathbf{p})$ is minimized with respect to the model parameters. By using the definition Eq. (33), the normalization parameters are adjusted implicitly. According to the theory of least-squares fitting, the expectation value of the minimum is $\langle \chi_{\min}^2 \rangle = N_{\text{df}} \pm \sqrt{2N_{\text{df}}}$, where N_{df} is the number of degrees of freedom, provided the data points are distributed statistically (*i.e.* they do not contain systematic errors) and provided they are Gaussian (which is the case for counting experiments with enough events per bin). The error matrix E of the model parameters is defined by

$$(E^{-1})_{\alpha\beta} = \frac{\partial^2 \chi^2(\mathbf{p})}{2\partial p_\alpha \partial p_\beta} \Big|_{\mathbf{p}=\mathbf{p}_{\min}}, \quad (34)$$

where \mathbf{p}_{\min} are the values of the model parameters in the minimum value of χ^2 . The error matrix allows us to determine the error in the model parameter p_α as $\sqrt{E_{\alpha\alpha}}$. This error corresponds to the variation in that parameter that gives a rise in χ_{\min}^2 of 1 when the remaining parameters are refitted. As mentioned in Sec. III, when the error is more than one third of the parameter value, it implies that χ_{\min}^2 rises by less than 9 when the remaining parameters are refitted. In that case the parameter is set to zero, *i.e.* it is left out. The error matrix allows us also to provide statistical uncertainties on our predictions for the observables. In the plots of the differential observables below, the PWA result is given as a full red line with an area bordered by blue dotted lines that indicate the one-standard-deviation uncertainty in the prediction.

TABLE III. Reference table of antiproton-proton scattering data with $p_{\text{lab}} \leq 923 \text{ MeV}/c$. The asterisks in the leftmost column indicate the data sets that were not included in Ref. [23], because the data are more recent or because the values of the data points were not available. The meanings of the superscripts in the heading and the comments in the rightmost column are given at the end of the table.

p_{lab} (MeV/c)	No. ^a type ^b	χ^2_{min}	Norm error ^v	Pred. norm ^c	Rejected ^d	Ref.	Comment
119.0–923.0	50 σ_{ce}	46.5	4%	1.058	$\leq 385.0, \# = 8; 468.0$	[45]	k, m
176.8–396.1	5 σ_{ann}	9.4	4.4%	0.949	176.8	[46]	
181.0	46 $d\sigma_{\text{el}}$.	5%	.	all	[47, 48]	j, l, o
183.0	13 $d\sigma_{\text{ce}}$	13.3	5%	1.002	0.940, $-0.170, -0.574$	[49]	
194.8	19 $d\sigma_{\text{el}}$.	4%	.	all	[50]	f, i, o
200.0–588.2	48 σ_{ann}	52.5	2.2%	0.989		[46, 51]	
221.9–413.2	45 σ_{tot}	55.3	∞	0.961	221.9, 229.6, 254.9, 260.8, 280.3, 289.1, 394.2, norm	[52]	
233.0	54 $d\sigma_{\text{el}}$.	5%	.	all	[53]	f, j
239.2	20 $d\sigma_{\text{el}}$	16.0	4%	1.077	-0.950	[50]	o
272.0	65 $d\sigma_{\text{el}}$	61.8	5%	1.005		[53]	j
276.0–922.0	21 σ_{ce}	26.2	7.5%	1.098		[54]	m
276.9	20 $d\sigma_{\text{el}}$	20.9	4%	1.027		[50]	o
287.0	54 $d\sigma_{\text{el}}$.	5%	.	all	[47, 48]	j, l, o
287.0	14 $d\sigma_{\text{ce}}$	29.6	5%	1.144		[49]	
310.4	20 $d\sigma_{\text{el}}$	30.6	4%	1.024		[50]	o
340.9	20 $d\sigma_{\text{el}}$	23.3	4%	1.033	$-0.950, -0.850$	[50]	o
348.7	38 $d\sigma_{\text{el}}$	40.9	4%	0.973		[55]	i, o
353.3	119 $d\sigma_{\text{el}}$	117.6	5%	1.007	0.366	[56]	j, o
355.0–923.0	36 σ_{tot}	.	1.5%	.	all	[57]	e, m
359.0–652.0*	11 $d\sigma_{\text{el}}$.	2%	.	all	[58]	t
369.1	19 $d\sigma_{\text{el}}$	16.0	4%	1.015	0.550	[50]	i, o
374.0	39 $d\sigma_{\text{el}}$	27.8	5%	1.040		[59]	o
388.0–598.6	29 σ_{tot}	35.2	∞	0.964	504.8, norm	[60]	
392.4	19 $d\sigma_{\text{el}}$.	5%	.	all	[61]	l

TABLE III. (*Continued*).

p_{lab} (MeV/ c)	No. ^a type ^b	χ^2_{min}	Norm error ^v	Pred. norm ^c	Rejected ^d	Ref.	Comment
392.4	15 $d\sigma_{\text{ce}}$	8.6	5%(6.4%)	1.103	0.985, 0.954, 0.244, 0.099, −0.059, −0.239, −0.616	[62]	w
395.9–737.4*	28 σ_{tot}	19.4	0.8%	1.007	737.4	[63, 64]	
404.3	38 $d\sigma_{\text{el}}$	36.3	4%	0.974		[55]	i, o
406.0–922.0	30 $d\sigma_{\text{el}}$	29.9	∞	0.757	norm	[65]	h, n
406.0	119 $d\sigma_{\text{el}}$	100.5	5%	1.002	0.991, 0.750, 0.579	[56]	j, o
411.2	38 $d\sigma_{\text{el}}$	33.0	5%	0.998	−0.875, −0.925	[59]	i, o
413.4	7 $d\sigma_{\text{el}}$	4.5	5%	1.043	0.992	[66]	j, o
424.5	7 $d\sigma_{\text{el}}$.	5%	.	all	[66]	e, j, o
428.0	10 $d\sigma_{\text{ce}}$	9.6	20%	1.170		[67]	
435.8	7 $d\sigma_{\text{el}}$	1.2	5%	1.007	0.992	[66]	j, o
439.0	27 $d\sigma_{\text{el}}$.	10%	.	all	[68]	l
439.0	24 $A_{y,\text{el}}$	36.0	∞	1.579		[68]	g, o
439.9	39 $d\sigma_{\text{el}}$	40.8	5%	1.006		[59]	o
440.8	38 $d\sigma_{\text{el}}$	48.7	5%	1.024	0.725	[59]	i, o
444.1	38 $d\sigma_{\text{el}}$	48.2	4%	0.967	−0.875	[55]	i, o
446.0	119 $d\sigma_{\text{el}}$	115.7	5%	0.998		[56]	j, o
447.1	7 $d\sigma_{\text{el}}$	6.1	5%	1.038	0.992	[66]	j, o
458.3	8 $d\sigma_{\text{el}}$	2.2	5%	0.986	0.996	[66]	j, o
467.5	39 $d\sigma_{\text{el}}$	31.3	4%	1.019	−0.925	[55]	i, o
467.8	39 $d\sigma_{\text{el}}$	23.5	5%	1.033		[59]	o
469.2	8 $d\sigma_{\text{el}}$	8.0	5%	1.004	0.996	[66]	j, o
479.3	119 $d\sigma_{\text{el}}$	109.5	5%	0.982	0.919, 0.873, 0.697	[56]	j, o
480.0	10 $d\sigma_{\text{ce}}$	10.1	∞	1.113		[69]	g
481.2	8 $d\sigma_{\text{el}}$	6.5	5%	1.037	0.996	[66]	j, o
490.1	37 $d\sigma_{\text{el}}$.	5%	.	all	[61]	l
490.1	15 $d\sigma_{\text{ce}}$	13.1	5%(6.9%)	1.001	0.992, −0.193, −0.381, −0.566	[62]	w
490.6	39 $d\sigma_{\text{el}}$	46.3	5%	0.963		[59]	o
492.7	8 $d\sigma_{\text{el}}$	3.9	5%	1.003	0.996	[66]	j, o
497.0	14 $A_{y,\text{el}}$	10.3	4.5%	1.004		[70, 71]	
498.7	37 $d\sigma_{\text{el}}$	28.4	4%	0.989		[55]	i, o
503.8	8 $d\sigma_{\text{el}}$	12.6	5%	1.034	0.996	[66]	j, o
504.7	39 $d\sigma_{\text{el}}$.	5%	.	all	[59]	e, o

TABLE III. (*Continued*).

p_{lab} (MeV/ c)	No. ^a type ^b	χ^2_{min}	Norm error ^v	Pred. norm ^c	Rejected ^d	Ref.	Comment
505.0	54 $d\sigma_{\text{el}}$.	5%	.	all	[47, 48]	j, l, o
505.0	14 $d\sigma_{\text{ce}}$	17.3	5%	1.021		[49]	
508.0	119 $d\sigma_{\text{el}}$	106.2	5%	0.998	0.663, 0.530	[56]	j, o
508.9	39 $d\sigma_{\text{el}}$	29.6	5%	1.005		[59]	o
516.0	8 $d\sigma_{\text{el}}$	5.1	5%	1.006	0.996	[66]	j, o
523.0	15 $A_{y,\text{el}}$	11.5	4.5%	1.037		[70, 71]	
524.8	36 $d\sigma_{\text{el}}$	32.2	4%	1.004		[55]	i, o
525.9	39 $d\sigma_{\text{el}}$	42.5	5%	1.033		[59]	o
528.2	8 $d\sigma_{\text{el}}$	2.9	5%	0.993	0.996	[66]	j, o
533.6	119 $d\sigma_{\text{el}}$	126.1	5%	1.012	0.892	[56]	j, o
537.0	10 $d\sigma_{\text{ce}}$	12.5	∞	1.179		[69]	g
540.6	8 $d\sigma_{\text{el}}$	10.7	5%	1.004	0.996	[66]	j, o
543.2	39 $d\sigma_{\text{el}}$	43.9	5%	1.051		[59]	o
544.0	33 $d\sigma_{\text{el}}$.	10%	.	all	[68]	l
544.0	30 $A_{y,\text{el}}$.	5%	.	all	[68]	f, g, o
546.0*	12 $d\sigma_{\text{ce}}$	12.7	15%	1.219		[72]	
546.0*	2 $d\sigma_{\text{ce}}$	1.0	15%	1.024		[72]	
546.0	23 $A_{y,\text{ce}}$	23.3	4%	0.966	-0.250	[73]	
546.0*	13 $A_{y,\text{ce}}$.	4%	.	all	[74]	f
546.0*	7 $D_{yy,\text{ce}}$	4.9	—	—		[74]	
549.4	10 $d\sigma_{\text{ce}}$	5.9	20%	1.219		[67]	
550.0	67 $d\sigma_{\text{el}}$	80.2	5%	0.978	0.997, 0.996, 0.995		
					0.910, 0.883	[75]	j
553.1	34 $d\sigma_{\text{el}}$	37.1	4%	0.967		[55]	i, o
553.4	8 $d\sigma_{\text{el}}$	2.2	5%	1.008	0.996, 0.972	[66]	j, o
556.9	119 $d\sigma_{\text{el}}$	124.1	5%	1.002	0.908	[56]	j, o
558.5	39 $d\sigma_{\text{el}}$	45.2	5%	1.021		[59]	o

TABLE III. (*Continued*).

p_{lab} (MeV/ c)	No. ^a type ^b	χ^2_{min}	Norm error ^v	Pred. norm ^c	Rejected ^d	Ref.	Comment
565.5	8 d σ_{el}	5.4	5%	0.994	0.996	[66]	j, o
568.4	37 d σ_{el}	35.4	5%	1.025	-0.675, -0.825	[59]	i, o
577.2	36 d σ_{el}	33.9	4%	0.969		[55]	i, o
578.1	9 d σ_{el}	6.0	5%	1.001	0.999	[66]	j, o
578.3	119 d σ_{el}	133.0	5%	1.022		[56]	j, o
584.0	10 d σ_{ce}	6.3	∞	1.043		[69]	g
590.0	39 d σ_{el}	.	5%	.	all	[47, 48]	j, l, o
590.0	15 d σ_{ce}	23.4	5%	1.030	0.996	[49]	
591.2	9 d σ_{el}	6.1	5%	1.016	0.999	[66]	j, o
591.2	39 d σ_{el}	.	5%	.	all	[61]	l
591.2	15 d σ_{ce}	11.3	5%(7.8%)	1.030	-0.358, -0.545	[62]	w
596.5	38 d σ_{el}	46.0	5%	1.059		[59]	o
599.2	33 d σ_{el}	15.8	4%	0.983		[55]	i, o
601.0*	47 d σ_{ce}	47.5	3%	1.035		[76]	
601.5*	47 d σ_{ce}	37.8	3%	1.074		[77]	
604.0	9 d σ_{el}	8.3	5%	0.975	0.999	[66]	j, o
615.0	38 d σ_{el}	55.0	5%	1.036		[59]	o
617.0	9 d σ_{el}	8.0	5%	0.944	0.998	[66]	j, o
630.0	10 d σ_{ce}	7.1	∞	1.046		[69]	g
630.9	9 d σ_{el}	4.5	5%	0.991	0.999	[66]	j, o
639.6	38 d σ_{el}	.	5%	.	all	[59]	e, o
644.7	9 d σ_{el}	9.2	5%	0.961	0.998	[66]	j, o
656.0*	10 d σ_{ce}	12.9	15%	1.220		[72]	
656.0*	7 d σ_{ce}	14.6	15%	1.165		[72]	
656.0	17 $A_{y,\text{ce}}$	11.2	4%	0.982		[78]	
656.0	21 $A_{y,\text{ce}}$	23.5	4%	0.956		[73]	
658.1	38 d σ_{el}	44.6	5%	0.963	0.225, -0.675	[59]	o

TABLE III. (*Continued*).

p_{lab} (MeV/ c)	No. ^a type ^b	χ^2_{min}	Norm error ^v	Pred. norm ^c	Rejected ^d	Ref.	Comment
658.6	9 $d\sigma_{\text{el}}$	8.9	5%	0.999	0.998	[66]	j, o
670.0	10 $d\sigma_{\text{ce}}$	6.2	∞	1.150		[69]	g
671.5	9 $d\sigma_{\text{el}}$	3.8	5%	0.981	0.998	[66]	j, o
679.0	26 $d\sigma_{\text{el}}$.	∞	.	all	[71]	h, l
679.0	27 $A_{y,\text{el}}$	25.1	4.5%	1.005	0.540	[70, 71]	
679.0	1 $D_{yy,\text{el}}$	3.2	—	—		[79]	q
679.1	4 $A_{y,\text{el}}$	4.1	5%	0.984		[80]	o
680.1	38 $d\sigma_{\text{el}}$	39.2	5%	0.990		[59]	o
686.1	9 $d\sigma_{\text{el}}$	4.3	5%	0.980	0.998	[66]	j, o
689.0	39 $d\sigma_{\text{el}}$.	5%	.	all	[61]	l
689.0	16 $d\sigma_{\text{ce}}$	17.9	5%(7.6%)	0.961	0.998, 0.981	[62]	w
690.0	89 $d\sigma_{\text{el}}$	94.5	4%	0.978	0.370	[81]	
693.0	24 $d\sigma_{\text{ce}}$	37.8	10%	1.103		[78]	r
693.0	17 $d\sigma_{\text{ce}}$	20.4	10%	1.041		[78]	r
696.1	21 $d\sigma_{\text{el}}$	18.5	4%	1.016		[82]	
696.1	16 $d\sigma_{\text{ce}}$	15.3	4%	1.031		[82]	
697.0	24 $d\sigma_{\text{el}}$.	10%	.	all	[83]	l
697.0	33 $A_{y,\text{el}}$	20.8	∞	1.213	0.629, norm	[83]	o
698.0	10 $d\sigma_{\text{ce}}$	7.0	∞	1.195		[69]	g
700.0	4 $A_{y,\text{el}}$	1.3	5%	0.997		[84]	o
701.1	9 $d\sigma_{\text{el}}$	3.8	5%	0.994	0.998	[66]	j, o
715.3	9 $d\sigma_{\text{el}}$	10.6	5%	0.997	0.998	[66]	j, o
728.0	10 $d\sigma_{\text{ce}}$	3.1	∞	1.065		[69]	g
730.0*	40 $d\sigma_{\text{ce}}$.	5%	.	all	[85]	f, s, u
757.0	72 $d\sigma_{\text{el}}$	81.4	5%	1.023	0.999, 0.997, 0.996, 0.991	[75]	j
760.0*	24 $d\sigma_{\text{ce}}$.	5%	.	all	[86]	f, s

TABLE III. (*Continued*).

p_{lab} (MeV/ c)	No. ^a type ^b	χ^2_{min}	Norm error ^v	Pred. norm ^c	Rejected ^d	Ref.	Comment
767.0*	10 $d\sigma_{\text{ce}}$	9.1	15%	1.441		[72]	
767.0*	8 $d\sigma_{\text{ce}}$	9.6	15%	1.231		[72]	
767.0	22 $A_{y,\text{ce}}$	28.0	4%	1.106		[73]	
780.5	39 $d\sigma_{\text{el}}$.	5%	.	all	[61]	l
780.5	15 $d\sigma_{\text{ce}}$	6.7	5%(7.1%)	0.963	0.982, -0.143	[62]	w
783.0	30 $d\sigma_{\text{el}}$.	∞	.	all	[71]	h, l
783.0	30 $A_{y,\text{el}}$	36.2	4.5%	1.068	$-0.300, -0.420$	[70, 71]	
783.0	3 $D_{yy,\text{el}}$	6.4	—	—		[79]	q
790.0	95 $d\sigma_{\text{el}}$	95.3	4%	1.020		[81]	
860.0	95 $d\sigma_{\text{el}}$	61.0	4%	1.019	0.510	[81]	
875.0*	10 $d\sigma_{\text{ce}}$	8.1	15%	1.366		[72]	
875.0*	10 $d\sigma_{\text{ce}}$	20.9	15%	1.183		[72]	
875.0*	12 $d\sigma_{\text{ce}}$	8.4	15%	1.417		[87]	
875.0	23 $A_{y,\text{ce}}$	12.1	4%	1.050		[73]	
875.0*	19 $A_{y,\text{ce}}$	19.2	4%	0.972		[87]	
875.0*	13 $A_{y,\text{ce}}$	14.0	15%	1.089		[87]	
875.0*	9 $D_{yy,\text{ce}}$	5.1	—	—		[74, 88]	q
875.0*	5 $K_{yy,\text{ce}}$	5.9	—	—		[89]	q
886.0	34 $d\sigma_{\text{el}}$.	∞	.	all	[71]	h, l
886.0	34 $A_{y,\text{el}}$	34.1	4.5%	1.023		[70, 71]	
886.0	1 $D_{yy,\text{el}}$	1.5	—	—		[79]	q
910.0	19 $d\sigma_{\text{el}}$.	∞	.	all	[90]	f, g
910.0	21 $A_{y,\text{el}}$	12.9	5%	0.990		[90]	

a The number includes all published data, except those given as 0.0 ± 0.0 (see Comment i), and those having $p_{\text{lab}} > 923$ MeV/ c (see Comment m).

b The subscripts “el” and “ce” denote observables in the elastic $\bar{p}p \rightarrow \bar{p}p$ and charge-

exchange $\bar{p}p \rightarrow \bar{n}n$ reactions, respectively. “ $d\sigma$ ” denotes a differential cross section $d\sigma/d\Omega$, “ A_y ” a polarization-type datum (asymmetry or analyzing power), “ D_{yy} ” a depolarization type datum, and “ K_{yy} ” a spin-transfer type datum. “ σ_{tot} ” stands for total cross section, “ σ_{ann} ” for total annihilation cross section, and “ σ_{ce} ” for total charge-exchange cross section.

- c Normalization, predicted by the analysis, with which the experimental values should be multiplied before comparison with the theoretical values.
- d Tabulated is p_{lab} in MeV/ c , $\cos\theta$, “norm” or “all.” The notation “ ≤ 385.0 , $\#=8$ ” e.g. means that the 8 points with $p_{\text{lab}} \leq 385.0$ MeV/ c are rejected. The “norm” means that the given normalization is rejected and a “floated” normalization is used instead. The “all” means that all of the data points in this set are rejected.
- e Group rejected due to improbable low χ_{min}^2 .
- f Group rejected due to improbable high χ_{min}^2 .
- g “Floated” normalization. Data are relative only.
- h Normalization “floated” by us, since the norm contributes much more than 9 to χ_{min}^2 .
- i Data points given as 0.0 ± 0.0 not included.
- j Coulomb-nuclear interference measurement. Data points in the extreme forward angular region are rejected when they contain multiple-scattering effects.
- k Data points at low momenta rejected.
- l Problematic differential cross sections. Not included in the database. For detailed explanation, see Sec. VIII B and Tables II and III of Ref. [23].
- m Part of a group of data with points having $p_{\text{lab}} > 923$ MeV/ c .
- n Elastic differential cross sections as a function of momentum taken at backward angle $\cos\theta = -0.994$.
- o Normalization error assumed by us, since no clear number is stated in the reference.
- p Depolarization data. Not included in the fit, in view of the large error bars.

- q Normalization error taken to be zero, in view of the large error bars of these data.
- r Data points taken at the same angles averaged.
- s Data taken from the website <http://hepdata.cedar.ac.uk>.
- t Data not available.
- u The momentum is the average of 700 MeV/ c and 760 MeV/ c .
- v Normalization errors as used in the fitting, as deduced from the experimental articles; when not explicitly given, a reasonable value was assumed by us.
- w The $x\%(y\%)$ notation means that $x\%$ is the overall normalization error and $y\%$ is the point-to-point systematic error.

The total χ^2_{\min} is only a global measure for the quality of the fit. In the Appendix, we discuss in more detail the statistical quality of the final database, by examining the final χ^2 distribution of the data points and how it compares to theoretical expectations.

Data selection is a necessary ingredient of a PWA. In PWAs of large amounts of scattering data, a significant minority of the data sets turns out to be inconsistent with the rest of the database and with the PWA solution. In these cases, the data sets usually suffer from large systematic errors, which cannot be traced and corrected for. Examples in our case are the elastic differential cross sections measured at LEAR, which are inconsistent among themselves and with earlier measurements, and which in many cases cannot even be fitted properly with Legendre polynomials, as discussed at length in Ref. [23]. Including these flawed data sets would seriously bias the PWA solution. To decide whether a data set or an individual data point is acceptable, we use the standard statistical criteria outlined in Ref. [25] and already applied in Ref. [23]. They are generalized three-sigma criteria: Any single data point with $\chi^2_{A,i} > 9$ is rejected, as well as any data set with significantly too high or too low χ^2_A , according to the limits given in Ref. [25]. Some data or data groups are rejected because of other reasons, as mentioned also in the Comments column of Table III.

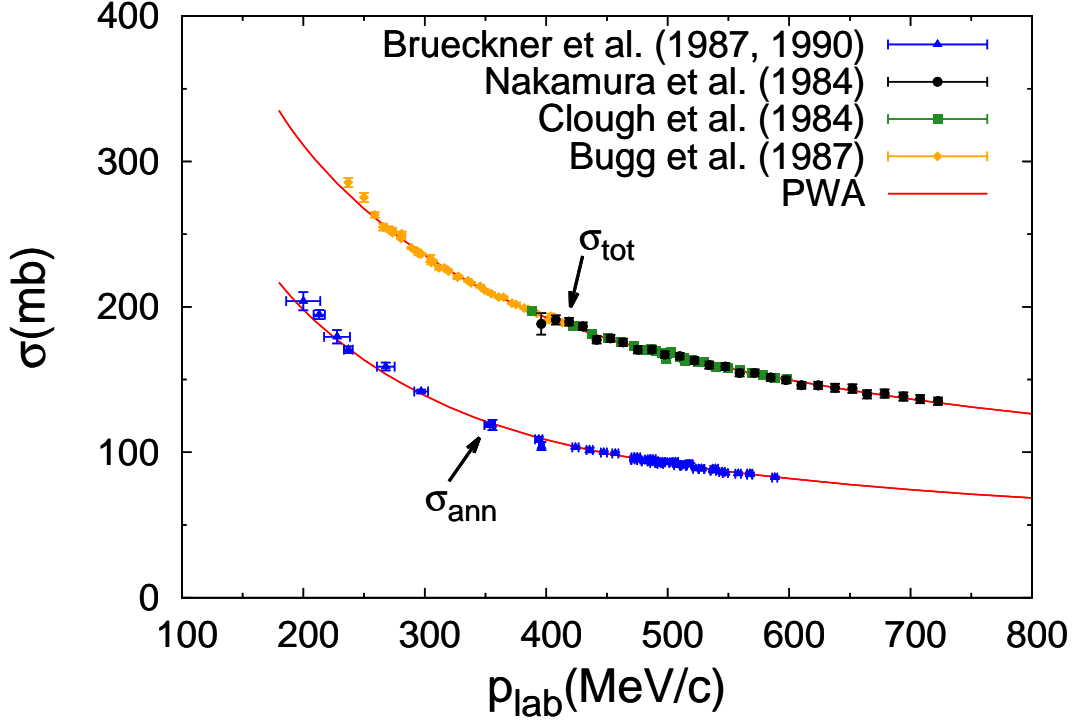


FIG. 2. (Color online) Total cross sections and total annihilation cross sections as function of antiproton laboratory momentum. The PWA fit has for Brückner *et al.* [46, 51] $\chi^2_{\min} = 9.4$ for 4 points σ_{ann} and $\chi^2_{\min} = 52.5$ for 48 points σ_{ann} ; for Nakamura *et al.* [64] $\chi^2_{\min} = 19.4$ for 27 points σ_{tot} ; for Clough *et al.* [60] $\chi^2_{\min} = 35.2$ for 28 points σ_{tot} ; for Bugg *et al.* [52] $\chi^2_{\min} = 55.3$ for 38 points σ_{tot} .

VI. DESCRIPTION OF THE DATA

The final $\bar{p}p$ database contains $N_{\text{obs}} = 3636$ scattering observables. The details for each of the data sets can be found in In Table III. We need $N_{\text{par}} = 46$ model (P -matrix) parameters for an optimal fit. In the fit we must determine at the same time N_n normalization parameters, so the total number of free parameters is $N_{\text{fp}} = N_{\text{par}} + N_n$. Of the N_n normalization parameters N_{ne} have a finite error, while the rest, $N_{\text{nf}} = N_n - N_{\text{ne}}$, is the number of “floated” normalizations. In our case, the total number of normalizations is 131, but we fixed the normalizations for the five depolarization D_{yy} and for the one spin transfer K_{yy} measurements, because these data sets have relatively large error bars. Therefore, $N_n = 125$. Of these, $N_{\text{nf}} = 12$ normalizations are “floated,” either because the data sets are relative

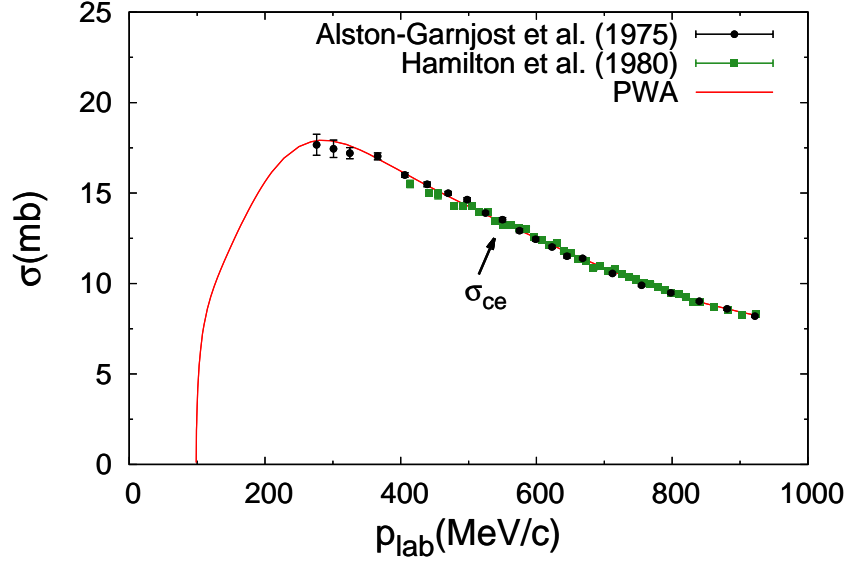


FIG. 3. (Color online) Total charge-exchange cross sections σ_{ce} as function of antiproton laboratory momentum. The PWA fit has for Alston-Garnjost *et al.* [54] $\chi^2_{\min} = 26.2$ for 21 points; for Hamilton *et al.* [45] $\chi^2_{\min} = 46.5$ for 41 points.

only, or because the normalization errors were underestimated in the experimental papers. Thus, the number of normalizations with errors is $N_{ne} = N_n - N_{nf} = 113$. This implies that the total number of free parameters is $N_{fp} = N_{par} + N_n = 171$, the total number of data is $N_{dat} = N_{obs} + N_{ne} = 3749$, and the number of degrees of freedom is $N_{df} = N_{dat} - N_{fp} = 3578$. The fit results in a minimum χ^2 value of $\chi^2_{\min} = 3750.6$. Therefore, the minimum χ^2 per datum is $\chi^2_{\min}/N_{dat} = 1.000$, and the minimum χ^2 per degree of freedom is $\chi^2_{\min}/N_{df} = 1.048$. When the model is perfect and the database is a perfect statistical ensemble, one expects $\langle \chi^2_{\min}/N_{df} \rangle = 1.000 \pm 0.024$, hence our result for χ^2_{\min}/N_{df} is only two standard deviations too high. The quality of the fit implies in particular that the charge-conjugated chiral OPE and TPE potential provides an excellent long-range \overline{NN} interaction.

A detailed discussion of most of the data sets can be found in Ref. [23]. Here we will show the results for a number of important data sets, and in particular address the high-quality data sets that were not available in Ref. [23]. The data sets in the figures have been multiplied by the predicted normalization factors given in Table III. The rejected outliers are not plotted in the figures. In case point-to-point systematic errors were added in quadrature to the statistical errors, we plot these total errors.

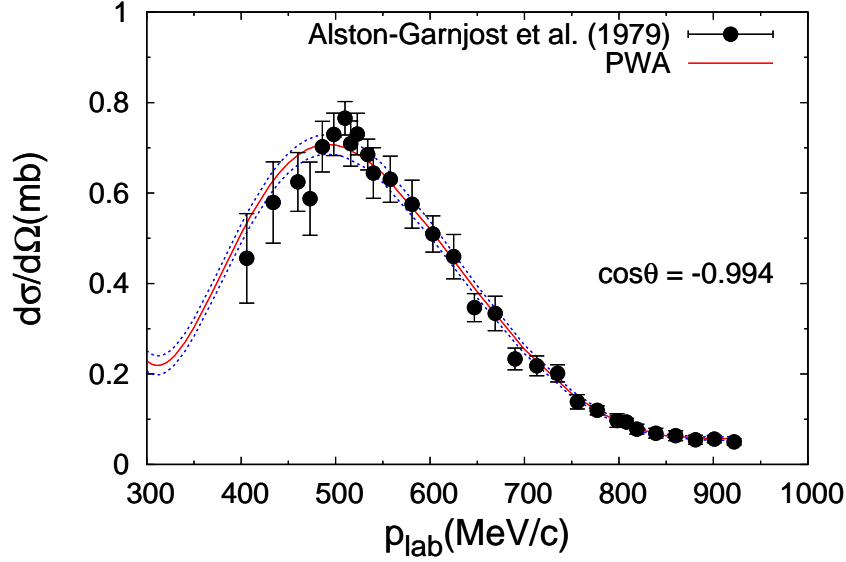


FIG. 4. (Color online) Elastic differential cross sections $d\sigma/d\Omega$ at backward angle, $\cos\theta = -0.994$, as function of antiproton laboratory momentum. The PWA result is given by the drawn red line and the dotted blue lines indicate the one-sigma uncertainty region. The fit has for Alston-Garnjost *et al.* [65] $\chi^2_{\min} = 29.9$ for 30 points.

In Fig. 2 the total cross sections σ_{tot} and the total annihilation cross sections σ_{ann} are plotted as function of p_{lab} , the antiproton momentum in the laboratory frame. For the annihilation cross sections, we introduced two different normalization parameters for the data taken with a thin and with a thick target, *cf.* Table III. In Fig. 3 the total charge-exchange cross sections σ_{ce} are plotted as function of p_{lab} . Unfortunately, there are no good data that map out the rise of the cross section above the $\bar{p}p \rightarrow \bar{n}n$ threshold at $p_{\text{lab}} \simeq 99$ MeV/ c . In Fig. 4 the elastic differential cross sections $d\sigma/d\Omega$ at backward angles with $\cos\theta = -0.994$ are plotted as function of the momentum in the laboratory frame. These data are described well, but the normalization of the data set was “floated.” At low energies, the theoretical uncertainty of the PWA is significantly smaller than the errors of the data points.

The partial-wave cross sections for both elastic and charge-exchange scattering at $p_{\text{lab}} = 200, 400, 600, \text{ and } 800$ MeV/ c are given in Table IV. It is clear that, in contrast to NN scattering, many partial waves contribute to $\bar{N}N$ scattering already at low energies. The reason is that the $\bar{N}N$ potentials, in particular the central and tensor components, are very

TABLE IV. Partial-wave elastic and charge-exchange cross sections, total cross sections, and total annihilation cross sections, in mb, for $p_{\text{lab}} = 200, 400, 600,$ and $800 \text{ MeV}/c$.

$p_{\text{lab}} \text{ (MeV}/c)$	$\bar{p}p \rightarrow \bar{p}p$				$\bar{p}p \rightarrow \bar{n}n$			
	200	400	600	800	200	400	600	800
1S_0	15.7	7.9	4.1	2.1	0.7	0.1		
1P_1	0.9	2.5	4.5	5.6	0.8	0.1		
1D_2	0.1	0.4	1.4	3.1	0.1	0.3	0.1	
1F_3		0.1	0.2	0.5		0.1	0.1	0.1
1G_4				0.1			0.1	0.1
3P_0	4.9	5.4	5.0	3.5	1.5	0.8	0.1	
3P_1	1.8	4.9	4.0	3.5	4.9	2.9	0.2	0.1
3D_2	0.1	0.3	1.0	1.5	0.3	2.4	2.5	1.0
3F_3		0.1	0.1	0.2		0.4	1.1	1.4
3G_4			0.1	0.1		0.1	0.3	0.5
3S_1	66.1	26.0	13.2	8.8	3.0	1.0	0.5	0.2
$^3S_1 \rightarrow ^3D_1$	0.3	0.4	0.2	0.1	0.8	1.5	1.1	0.6
$^3D_1 \rightarrow ^3S_1$	0.3	0.4	0.2	0.1	2.0	2.0	1.2	0.7
3D_1	0.1	0.5	0.8	1.0	0.1	0.5	0.6	0.4
3P_2	7.0	17.0	13.9	9.6	0.9	1.4	0.4	0.1
$^3P_2 \rightarrow ^3F_2$	0.1	0.1	0.1		0.1	0.5	0.5	0.5
$^3F_2 \rightarrow ^3P_2$	0.1	0.1	0.1		0.3	0.8	0.6	0.5
3F_2			0.1	0.4			0.1	0.1
3D_3		1.6	5.9	7.0		0.5	1.3	0.6
$^3D_3 \rightarrow ^3G_3$		0.1	0.1			0.2	0.3	0.3
$^3G_3 \rightarrow ^3D_3$		0.1	0.1			0.3	0.5	0.4
3G_3								0.1
3F_4			0.3	0.8			0.1	0.3
$^3F_4 \rightarrow ^3H_4$				0.1			0.2	0.2
$^3H_4 \rightarrow ^3F_4$				0.1		0.1	0.2	0.3
3H_4								
Rest			0.1	0.3		0.1	0.4	0.8
Singlet	16.7	10.9	10.2	11.3	1.6	0.6	0.4	0.3
Triplet	80.8	56.9	45.1	37.1	14.0	15.6	12.1	9.2
Total	97.5	67.9	55.3	48.4	15.6	16.2	12.5	9.4
$p_{\text{lab}} \text{ (MeV}/c)$	$\bar{p}p \rightarrow \text{all}$				$\bar{p}p \rightarrow \text{mesons}$			
	200	400	600	800	200	400	600	800
	311.2	192.6	149.8	126.4	198.1	108.5	81.9	68.6

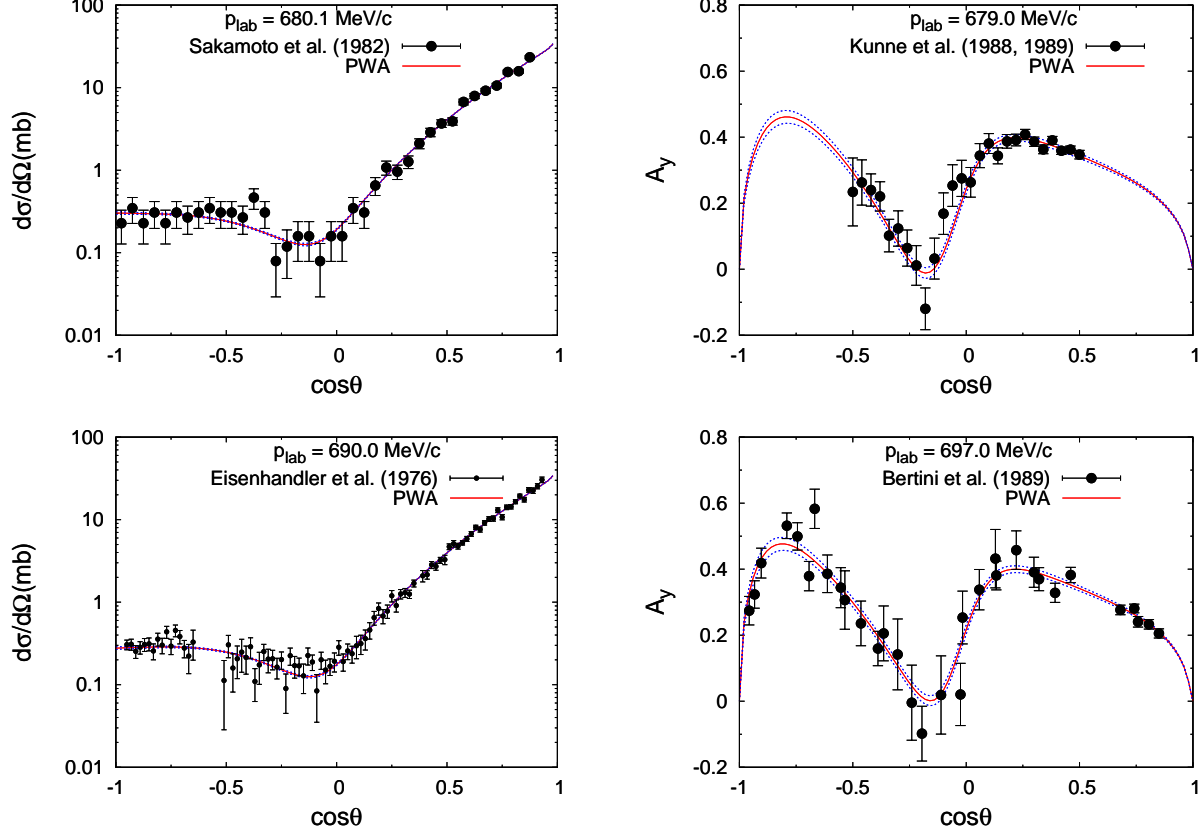


FIG. 5. (Color online) Differential cross sections and analyzing powers for elastic scattering as function of angle in the center-of-mass system. The PWA result is given by the drawn red line and the dotted blue lines indicate the one-sigma uncertainty region. The fit has for Sakamoto *et al.* [59] $\chi^2_{\min} = 39.2$ for 38 points $d\sigma/d\Omega$; for Kunne *et al.* [70, 71] $\chi^2_{\min} = 25.1$ for 26 points A_y ; for Eisenhandler *et al.* [81] $\chi^2_{\min} = 94.5$ for 88 points $d\sigma/d\Omega$; for Bertini *et al.* [83] $\chi^2_{\min} = 20.8$ for 32 points A_y .

strong. The dominance of the tensor force is seen in particular in the charge-exchange $\bar{p}p \rightarrow \bar{n}n$ reaction. For low energies of the final-state $\bar{n}n$ system the strong tensor force leads to large cross sections for the transitions $\ell(\bar{n}n) = \ell(\bar{p}p) - 2$, in particular ${}^3D_1 \rightarrow {}^3S_1$ and ${}^3F_2 \rightarrow {}^3P_2$. This is similar to the strangeness-exchange reaction $\bar{p}p \rightarrow \bar{\Lambda}\Lambda$, where these off-diagonal tensor-force transitions due to $K(494)$ and $K^*(892)$ exchange dominate the cross section in the $\bar{\Lambda}\Lambda$ threshold region [43, 44]. For these transitions, there is a large overlap between the wave functions of the initial $\bar{p}p$ state and the final $\bar{n}n$ or $\bar{\Lambda}\Lambda$ state [44] at low energy. The contributions from the spin-triplet states are much larger than the contributions from the spin-singlet states, especially for $\bar{p}p \rightarrow \bar{n}n$. The total annihilation cross section is

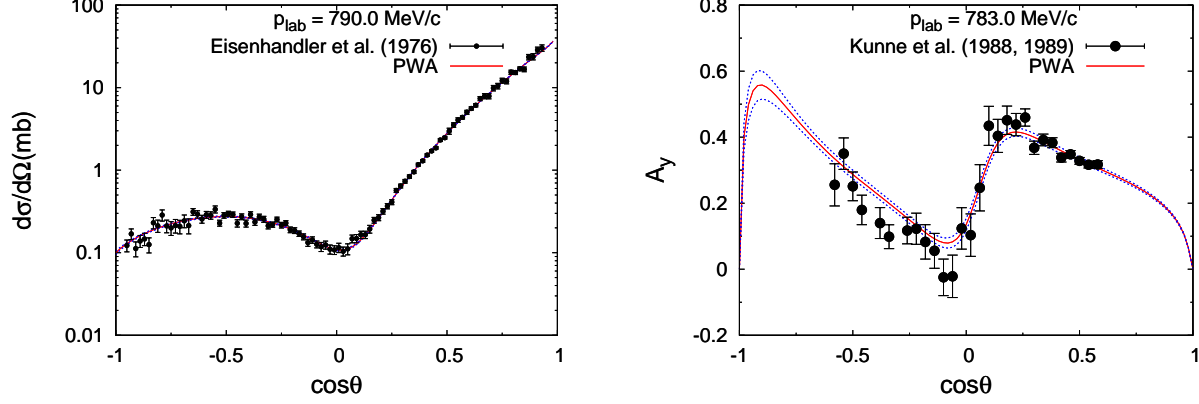


FIG. 6. (Color online) Differential cross sections and analyzing powers for elastic scattering as function of angle in the center-of-mass system. The PWA result is given by the drawn red line and the dotted blue lines indicate the one-sigma uncertainty region. The fit has for Eisenhandler *et al.* [81] $\chi^2_{\min} = 95.3$ for 95 points $d\sigma/d\Omega$; for Kunne *et al.* [70, 71] $\chi^2_{\min} = 36.2$ for 28 points A_y .

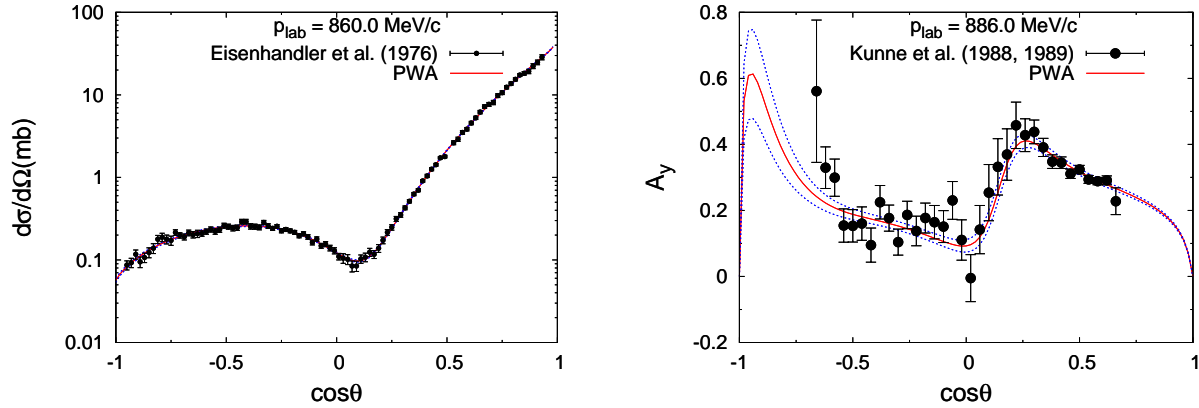


FIG. 7. (Color online) Differential cross sections and analyzing powers for elastic scattering as function of angle in the center-of-mass system. The PWA result is given by the drawn red line and the dotted blue lines indicate the one-sigma uncertainty region. The fit has for Eisenhandler *et al.* [81] $\chi^2_{\min} = 61.0$ for 94 points $d\sigma/d\Omega$; for Kunne *et al.* [70, 71] $\chi^2_{\min} = 34.1$ for 34 points A_y .

large, and decreases from a fraction of about 2/3 of the total cross section at $p_{\text{lab}} = 200$ MeV/ c to about 1/2 of the total cross section at $p_{\text{lab}} = 800$ MeV/ c .

In Figs. 5, 6, and 7 the differential cross sections $d\sigma/d\Omega$ and the analyzing powers A_y are shown for elastic scattering $\bar{p}p \rightarrow \bar{p}p$ at momenta near 690, 790, and 860 MeV/ c , respectively. In general, the uncertainty on the PWA prediction for the differential cross sections is

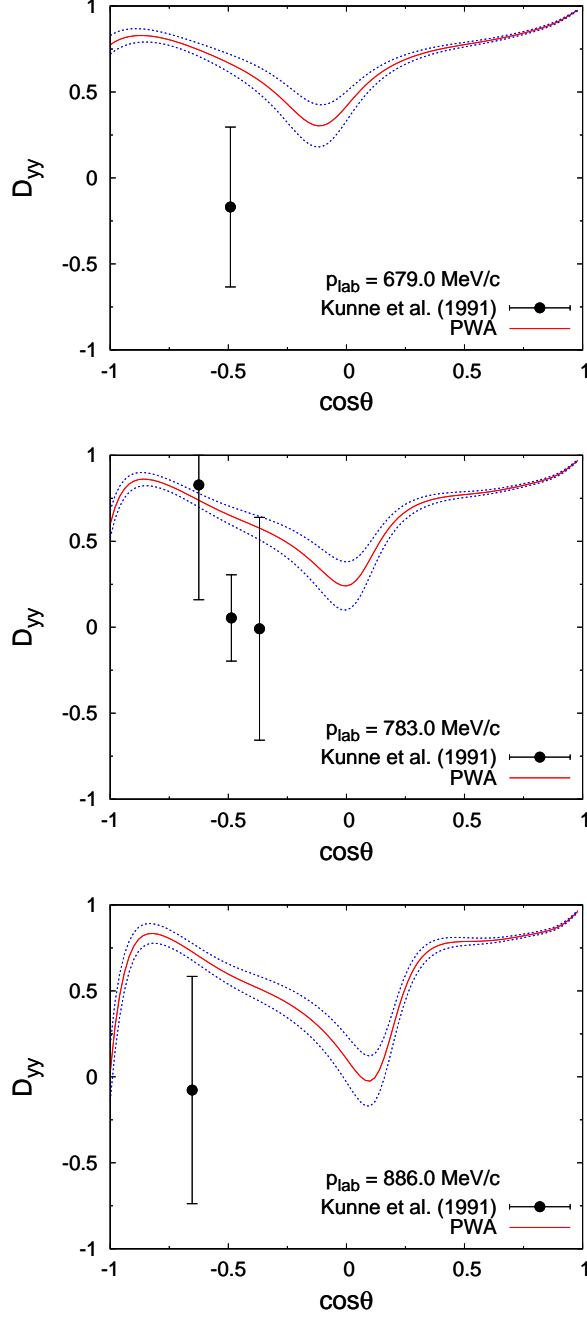


FIG. 8. (Color online) Differential depolarizations D_{yy} for elastic scattering as function of angle in the center-of-mass system. The PWA result is given by the drawn red line and the dotted blue lines indicate the one-sigma uncertainty region. The fit has for Kunne *et al.* [79] at $p_{\text{lab}} = 679.0 \text{ MeV}/c$ $\chi^2_{\text{min}} = 3.2$ for 1 point, at $p_{\text{lab}} = 783.0 \text{ MeV}/c$ $\chi^2_{\text{min}} = 6.4$ for 3 points, at $p_{\text{lab}} = 886.0 \text{ MeV}/c$ $\chi^2_{\text{min}} = 1.5$ for 1 point.

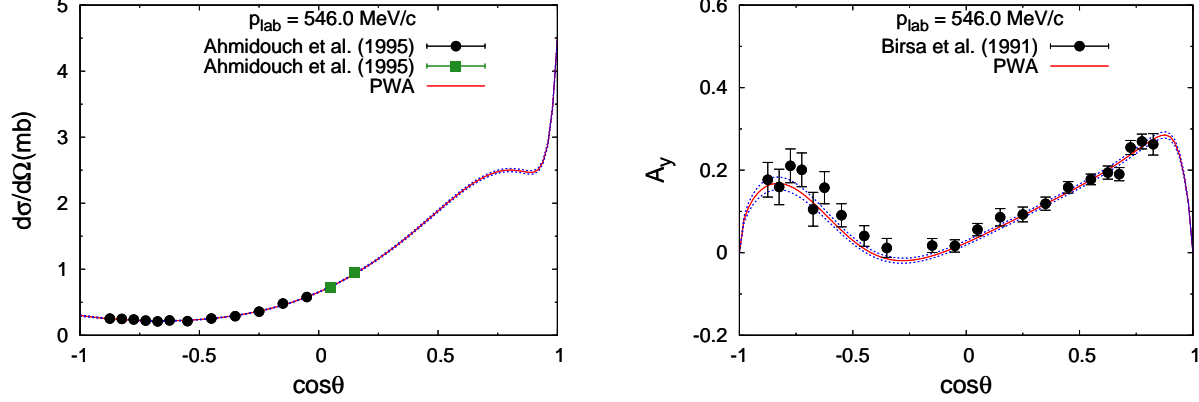


FIG. 9. (Color online) Differential cross sections and analyzing powers for charge-exchange scattering as function of angle in the center-of-mass system. The PWA result is given by the drawn red line and the dotted blue lines indicate the one-sigma uncertainty region. The fit has for Ahmidouch *et al.* [72] $\chi^2_{\min} = 12.7$ for 12 points $d\sigma/d\Omega$ at backward angles, $\chi^2_{\min} = 1.0$ for 2 points $d\sigma/d\Omega$ at forward angles; for Birsa *et al.* [73] $\chi^2_{\min} = 23.3$ for 22 points A_y .

determined by the accuracy of the data. For the analyzing powers, on the other hand, the theoretical uncertainties are in general smaller than the errors of the data points. The theoretical uncertainty is very small for forward angles. For backward angles, where there are no data available, this uncertainty increases. Fig. 8 shows the very limited data available for the depolarization D_{yy} for elastic scattering at 679, 783, and 886 MeV/c. There are only a few data points in the backward hemisphere and the data points have large error bars. In this case, the theoretical uncertainty for the PWA prediction is much smaller than these error bars, which implies that there is little new information in these data and that the fit would not change significantly if they were left out of the fit. The theoretical uncertainty is again very small for forward angles.

Figs. 9, 10, 11, and 12 show the differential cross sections $d\sigma/d\Omega$ and the analyzing powers A_y for charge-exchange scattering $\bar{p}p \rightarrow \bar{n}n$ at 546, 656, 767, and 875 MeV/c, respectively. Like for the elastic case, one observes that, in general, the uncertainty on the PWA prediction for the differential cross sections is determined by the accuracy of the data. For the analyzing powers, on the other hand, the theoretical uncertainties are in general smaller than the errors of the data points. For some of the differential cross-section measurements, we introduced different normalization parameters for the data in the forward

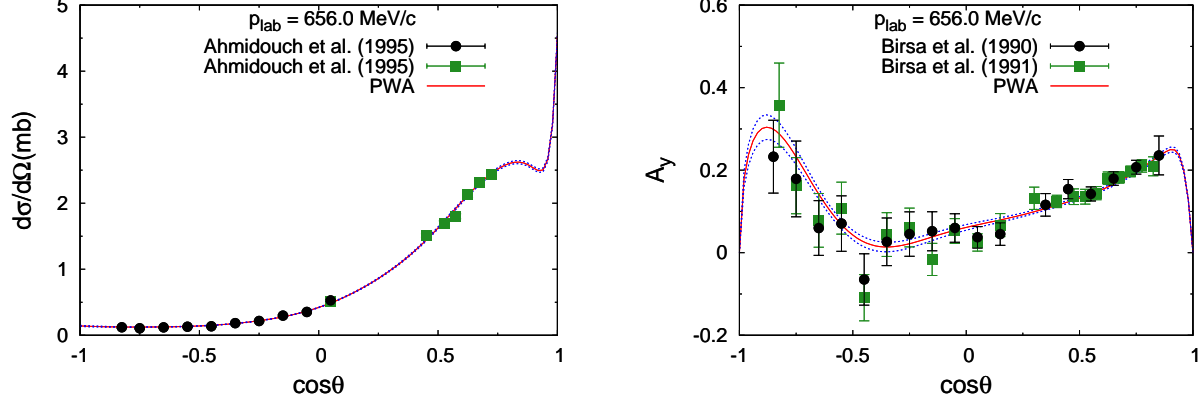


FIG. 10. (Color online) Differential cross sections and analyzing powers for charge-exchange scattering as function of angle in the center-of-mass system. The PWA result is given by the drawn red line and the dotted blue lines indicate the one-sigma uncertainty region. The fit has for Ahmidouch *et al.* [72] $\chi^2_{\min} = 12.9$ for 10 points $d\sigma/d\Omega$ at backward angles, $\chi^2_{\min} = 14.6$ for 7 points $d\sigma/d\Omega$ at forward angles; for Birsa *et al.* [78] $\chi^2_{\min} = 11.2$ for 17 points A_y ; for Birsa *et al.* [73] $\chi^2_{\min} = 23.5$ for 21 points A_y .

and in the backward hemisphere, which were taken with different detectors. The charge-exchange differential cross section is highly anisotropic, because of the contributions of many, high- ℓ partial waves. It has a “spike” at the most forward angles and it is flat at backward angles. It exhibits a very typical dip-bump structure at forward angles, which is due to the interference of the OPE interaction with a background due to short-range interactions [91]. The precise form of this structure evolves rapidly as function of energy, from a rather flat plateau structure at 546 MeV/ c to a pronounced dip-bump structure at 875 MeV/ c . The structure was measured accurately at 601 MeV/ c by the PS206 experiment at the end of the LEAR era [76, 77]. The high-quality charge-exchange differential cross sections from Ref. [77] are shown in Fig. 13. At the time of Ref. [23], only the data at 693 MeV/ c shown in Fig. 13 were available [78], but these differential cross sections did not pin down the dip-bump structure. The PWA of Ref. [23] predicted a more pronounced structure for this data set.

In Fig. 14 the few data sets available for the depolarization D_{yy} at 546 and 875 MeV/ c and the spin transfer K_{yy} at 875 MeV/ c in charge-exchange scattering are shown. The data points have large error bars, and also in this case the theoretical uncertainty for the PWA

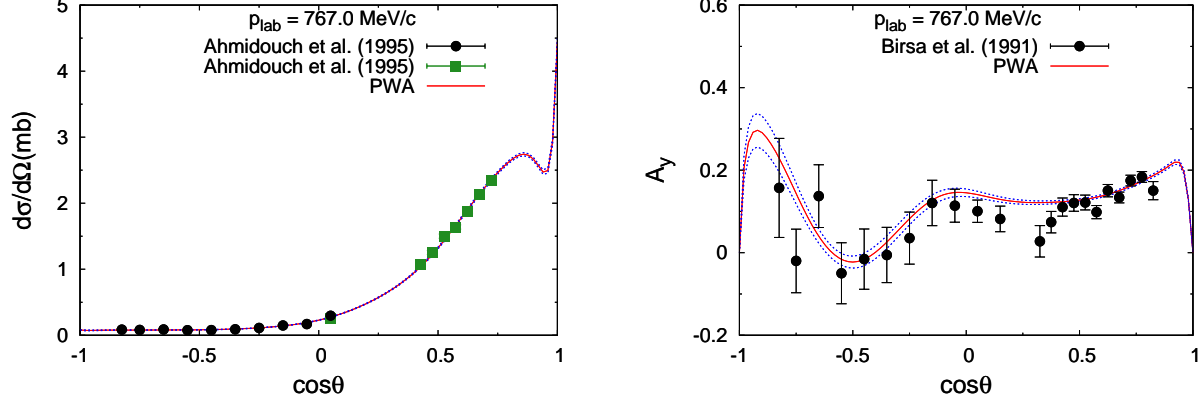


FIG. 11. (Color online) Differential cross sections and analyzing powers for charge-exchange scattering as function of angle in the center-of-mass system. The PWA result is given by the drawn red line and the dotted blue lines indicate the one-sigma uncertainty region. The fit has for Ahmidouch *et al.* [72] $\chi^2_{\min} = 9.1$ for 10 points $d\sigma/d\Omega$ at backward angles, $\chi^2_{\min} = 9.6$ for 8 points $d\sigma/d\Omega$ at forward angles; for Birsa *et al.* [73] $\chi^2_{\min} = 28.0$ for 22 points A_y .

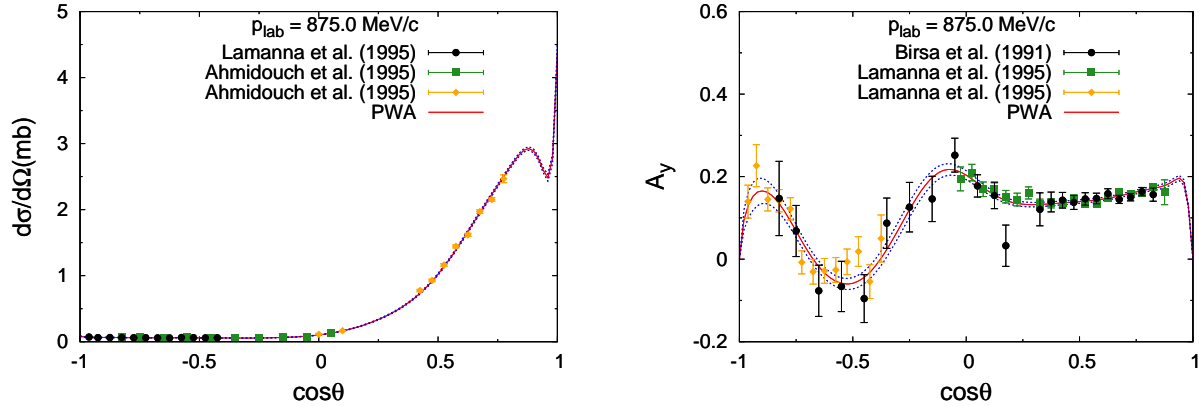


FIG. 12. (Color online) Differential cross sections and analyzing powers for charge-exchange scattering as function of angle in the center-of-mass system. The PWA result is given by the drawn red line and the dotted blue lines indicate the one-sigma uncertainty region. The fit has for Lamanna *et al.* [87] $\chi^2_{\min} = 8.4$ for 12 points $d\sigma/d\Omega$; for Ahmidouch *et al.* [72] $\chi^2_{\min} = 8.1$ for 10 points $d\sigma/d\Omega$ at backward angles, $\chi^2_{\min} = 20.9$ for 10 points $d\sigma/d\Omega$ at forward angles; for Birsa *et al.* [73] $\chi^2_{\min} = 12.1$ for 23 points A_y ; for Lamanna *et al.* [87] $\chi^2_{\min} = 19.2$ for 19 points A_y at forward angles, $\chi^2_{\min} = 14.0$ for 13 points A_y at backward angles.

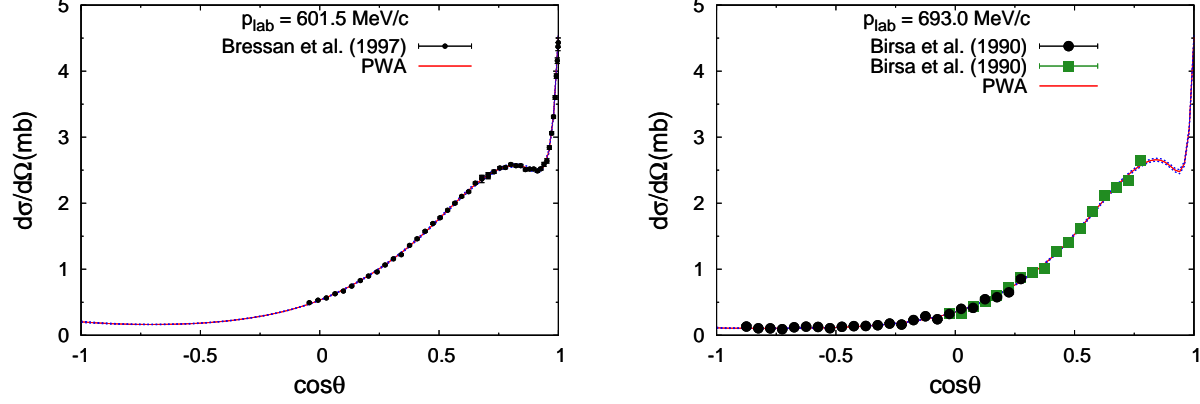


FIG. 13. (Color online) Differential cross sections $d\sigma/d\Omega$ for charge-exchange scattering as function of angle in the center-of-mass system. The PWA result is given by the drawn red line and the dotted blue lines indicate the one-sigma uncertainty region. The fit has for Bressan *et al.* [77] $\chi^2_{\min} = 37.8$ for 47 points; for Birsa *et al.* [78] $\chi^2_{\min} = 37.8$ for 24 points at backward angles, $\chi^2_{\min} = 20.4$ for 17 points at forward angles.

prediction is much smaller than these error bars. This demonstrates that spin observables are, of course, important, but they improve a good energy-dependent PWA only if they are precise enough [24]. The theoretical uncertainty is again very small for forward angles.

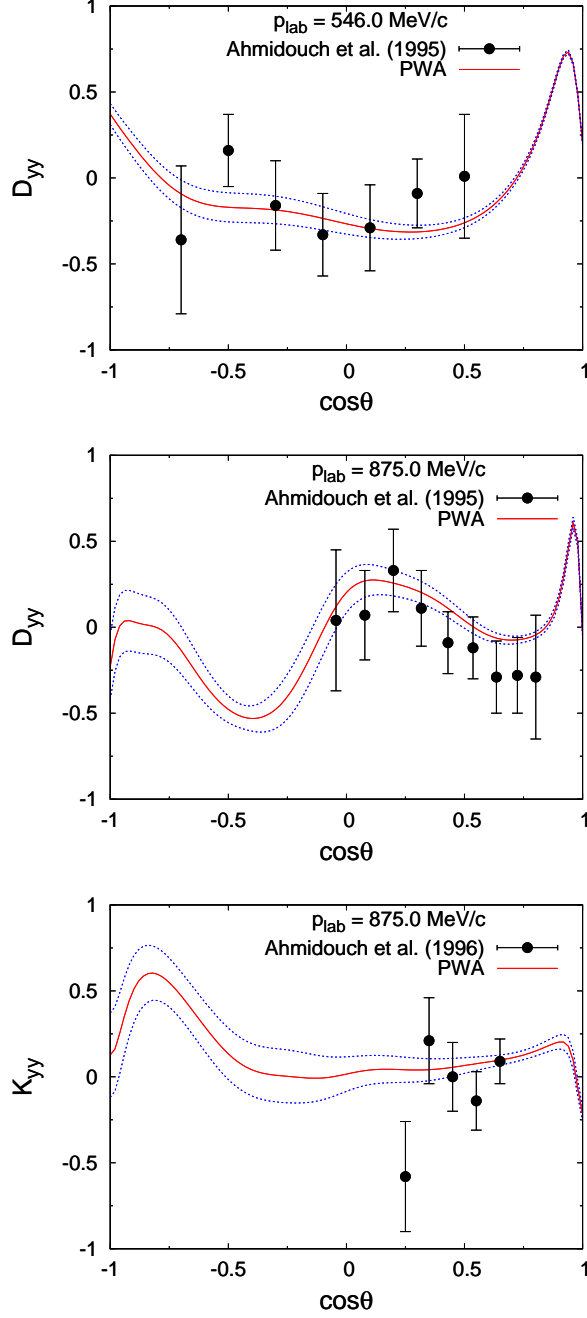


FIG. 14. (Color online) Differential depolarizations and spin transfers for charge-exchange scattering as function of angle in the center-of-mass system. The PWA result is given by the drawn red line and the dotted blue lines indicate the one-sigma uncertainty region. The fit has for Ahmidouch *et al.* [74] at $p_{\text{lab}} = 546.0 \text{ MeV}/c$ $\chi^2_{\text{min}} = 4.9$ for 7 points D_{yy} ; for Ahmidouch *et al.* [74] (Birsa *et al.* [88]) at $p_{\text{lab}} = 875.0 \text{ MeV}/c$ $\chi^2_{\text{min}} = 5.1$ for 9 points D_{yy} ; for Ahmidouch *et al.* [89] at $p_{\text{lab}} = 875.0 \text{ MeV}/c$ $\chi^2_{\text{min}} = 5.9$ for 5 points K_{yy} .

VII. PHASE-SHIFT AND INELASTICITY PARAMETERS

In this section we present results for the $\bar{N}N$ S matrix. The S matrix for the coupled $\bar{p}p$ and $\bar{n}n$ channels from our PWA suffices to construct the complete scattering amplitudes and hence the observables. For the uncoupled partial waves with $\ell = J$, $s = 0, 1$ or $\ell = 1$, $J = 0$, the S matrix is 2×2 , while for the coupled partial waves with $\ell = J \pm 1$ ($J \geq 1$), $s = 1$, it is a 4×4 matrix. We give numerical values at a number of momenta. Other results are available upon request. The matrix elements of S_{C+N}^C for different partial waves for the elastic and charge-exchange reactions are given in Tables V, VI, and VII for $p_{\text{lab}} = 100$ to 1000 MeV/ c . The S matrices are symmetric for the coupled partial waves in the case of elastic $\bar{p}p$ and $\bar{n}n$ scattering, but they are not symmetric in the case of charge-exchange scattering $\bar{p}p \leftrightarrow \bar{n}n$, as one can see from Table VI for $\bar{p}p \rightarrow \bar{p}p$ and from Table VII for $\bar{p}p \rightarrow \bar{n}n$.

For illustrative purposes we also present phase-shift and inelasticity parameters assuming that isospin symmetry is exact (we take then the average nucleon and pion mass and set the electromagnetic interaction to zero). In that case, the parametrization of the S matrix can be done in a transparent way, similar to the procedures used for NN scattering (above the pion-production threshold).

For the uncoupled partial waves with $\ell = J$, $s = 0, 1$ or $\ell = 1$, $J = 0$, the S matrix, for isospin $I = 0$ or $I = 1$, is a 1×1 matrix that can be written as

$$S^J = \eta \exp(2i\delta) , \quad (35)$$

where δ is the phase shift and η ($0 \leq \eta \leq 1$) is the inelasticity due to the annihilation into mesonic channels. The S matrix for the uncoupled waves is thus given in terms of two parameters, which are functions of energy. For high values of ℓ , where there is almost no annihilation, $\eta \rightarrow 1$.

For the partial waves with $\ell = J \pm 1$ ($J \geq 1$), $s = 1$, coupled by a tensor force, the S -matrix, for isospin $I = 0$ or $I = 1$, is a 2×2 matrix that can be parametrized by the generalized “bar-phase” convention [92]

$$S^J = \exp(i\bar{\delta}) \exp(i\bar{\epsilon}_J \sigma_x) H^J \exp(i\bar{\epsilon}_J \sigma_x) \exp(i\bar{\delta}) , \quad (36)$$

where $\bar{\delta}$ is a 2×2 diagonal matrix with real entries $\bar{\delta}_{J-1,J}$ and $\bar{\delta}_{J+1,J}$, and $\bar{\epsilon}_J$ is the mixing angle for the coupled partial waves; σ_x is the first Pauli matrix. The matrix H^J is used to

parametrize the inelasticity. Different ways to write H^J can be found in the literature. We will follow the parametrization of Ref. [93], in which one writes

$$H^J = \exp(-i\omega_J \sigma_y) \begin{pmatrix} \eta_{J-1,J} & 0 \\ 0 & \eta_{J+1,J} \end{pmatrix} \exp(i\omega_J \sigma_y) , \quad (37)$$

where $\eta_{J-1,J}$ and $\eta_{J+1,J}$ are real numbers with $0 \leq \eta_{J\mp 1,J} \leq 1$, and ω_J is the mixing angle for the inelasticity; σ_y is the second Pauli matrix. The S matrix for these coupled waves is thus given in terms of six parameters.

From the numerical results of the PWA, one has to extract for each energy the phase-shift and inelasticity parameters from the numerical values of the S matrix. For the uncoupled partial waves this is easy. In order to obtain the phase-shift and inelasticity parameters for the coupled partial waves, the algorithm of Ref. [92] is used. One can write the S matrix as

$$S^J = \begin{pmatrix} R_{11} \exp(2i\delta_{11}) & iR_{12} \exp(2i\delta_{12}) \\ iR_{12} \exp(2i\delta_{12}) & R_{22} \exp(2i\delta_{22}) \end{pmatrix} , \quad (38)$$

where R_{ij} and δ_{ij} are real numbers. When one defines the auxiliary phases

$$\begin{aligned} \theta_a &\equiv \delta_{11} - \bar{\delta}_{J-1,J} , \\ \theta_b &\equiv \delta_{22} - \bar{\delta}_{J+1,J} , \\ \delta' &\equiv \delta_{11} + \delta_{22} - 2\delta_{12} , \end{aligned} \quad (39)$$

it follows that

$$\begin{aligned} \tan 2(\theta_a + \theta_b) &= \frac{R_{12}^2 \sin 2\delta'}{R_{11}R_{22} + R_{12}^2 \cos 2\delta'} , \\ \tan(\theta_a - \theta_b) &= \frac{R_{22} - R_{11}}{R_{11} + R_{22}} \tan(\theta_a + \theta_b) . \end{aligned} \quad (40)$$

From this the phase-shift parameters $\bar{\delta}_{J-1,J}$ and $\bar{\delta}_{J+1,J}$ can be obtained. The mixing angle $\bar{\varepsilon}_J$ is given by

$$\tan 2\bar{\varepsilon}_J = \frac{2R_{12} \cos(\theta_a + \theta_b - \delta')}{R_{11} \cos 2\theta_a + R_{22} \cos 2\theta_b} . \quad (41)$$

The elements of the matrix H^J can then be related to the parameters obtained. One finds

$$\begin{aligned} 2H_{11} \cos 2\bar{\varepsilon}_J &= R_{11}(1 + \cos 2\bar{\varepsilon}_J) \cos 2\theta_a + R_{22}(1 - \cos 2\bar{\varepsilon}_J) \cos 2\theta_b , \\ 2H_{22} \cos 2\bar{\varepsilon}_J &= R_{11}(1 - \cos 2\bar{\varepsilon}_J) \cos 2\theta_a + R_{22}(1 + \cos 2\bar{\varepsilon}_J) \cos 2\theta_b , \\ H_{12} \cos 2\bar{\varepsilon}_J &= R_{12} \sin(\delta' - \theta_a - \theta_b) , \end{aligned} \quad (42)$$

from which one can determine the values of H_{11} , H_{22} , and H_{12} . By using Eq. (37), the remaining parameters $\eta_{J-1,J}$, $\eta_{J+1,J}$, and ω_J can be obtained via

$$\begin{aligned}\eta_{J-1,J} + \eta_{J+1,J} &= \text{Tr } H^J , \\ \eta_{J-1,J} \eta_{J+1,J} &= \det H^J , \\ \tan 2\omega_J &= 2H_{12}/(H_{11} - H_{22}) .\end{aligned}\tag{43}$$

If one extracts the values of the parameters for one single energy, there can be ambiguities [24]. In order to ensure continuity as function of energy one can always change the values of these parameters in such a way that the corresponding S -matrix elements are not changed. In the case of uncoupled partial waves, one can change δ by 180° and keep η unchanged, as can be seen from Eq. (35). In the case of the coupled partial waves, for instance, one can change $\bar{\delta}_{J-1,J}$ or $\bar{\delta}_{J+1,J}$ by 180° and at the same time change the signs of $\bar{\varepsilon}_J$ and ω_J , while keeping $\eta_{J-1,J}$ and $\eta_{J+1,J}$ unchanged; one can also change both $\bar{\delta}_{J-1,J}$ and $\bar{\delta}_{J+1,J}$ by 180° at the same time and keep $\eta_{J-1,J}$, $\eta_{J+1,J}$, $\bar{\varepsilon}_J$, and ω_J unchanged. In the limit where $\eta_{J\mp 1,J} = 1$, $\bar{\delta}_{J\mp 1,J} = 0$, and $\bar{\varepsilon}_J = 0$, one can choose $\omega_J = 0$ in order to keep continuity, although ω_J can take any value in this case, but the corresponding S -matrix elements are unchanged.

The results of the phase-shift and inelasticity parameters are given in Tables VIII, IX, and X for $p_{\text{lab}} = 100$ to 1000 MeV/ c . A convenient way to plot the S matrix, or equivalently $T = (S - 1)/i$, as function of energy is to use Argand diagrams. In Fig. 15 Argand diagrams are shown for the uncoupled partial waves and in Fig. 16 for the coupled ones assuming isospin symmetry.

TABLE V. S -matrix elements of the uncoupled partial waves for $\bar{p}p \rightarrow \bar{p}p$ and $\bar{p}p \rightarrow \bar{n}n$.

$p_{\text{lab}}(\text{MeV}/c)$	100	200	300	400	500	
$\bar{p}p \rightarrow \bar{p}p$	1S_0	$0.596 - 0.193i$	$0.351 - 0.296i$	$0.162 - 0.300i$	$0.032 - 0.242i$	$-0.033 - 0.157i$
	3P_0	$0.883 - 0.023i$	$0.657 - 0.199i$	$0.450 - 0.287i$	$0.216 - 0.248i$	$-0.007 - 0.145i$
	1P_1	$0.987 + 0.023i$	$0.916 + 0.054i$	$0.806 + 0.015i$	$0.688 - 0.076i$	$0.563 - 0.181i$
	3P_1	$0.989 - 0.030i$	$0.898 - 0.093i$	$0.745 - 0.173i$	$0.618 - 0.238i$	$0.524 - 0.253i$
	1D_2	$1.000 + 0.002i$	$0.996 + 0.020i$	$0.977 + 0.050i$	$0.925 + 0.074i$	$0.835 + 0.072i$
	3D_2	$1.000 - 0.003i$	$0.998 - 0.025i$	$0.981 - 0.050i$	$0.938 - 0.064i$	$0.869 - 0.071i$
	1F_3	$1.000 + 0.000i$	$1.000 + 0.004i$	$0.999 + 0.015i$	$0.997 + 0.031i$	$0.989 + 0.051i$
	3F_3	$1.000 + 0.000i$	$1.000 - 0.006i$	$0.999 - 0.021i$	$0.995 - 0.039i$	$0.985 - 0.052i$
	1G_4	$1.000 + 0.000i$	$1.000 + 0.001i$	$1.000 + 0.005i$	$1.000 + 0.012i$	$0.999 + 0.020i$
	3G_4	$1.000 + 0.000i$	$1.000 - 0.001i$	$1.000 - 0.008i$	$0.999 - 0.018i$	$0.998 - 0.030i$
$\bar{p}p \rightarrow \bar{n}n$	1S_0	$-0.021 + 0.090i$	$0.068 + 0.131i$	$0.100 + 0.035i$	$0.070 - 0.041i$	$0.009 - 0.077i$
	3P_0	$-0.007 + 0.002i$	$-0.220 - 0.020i$	$-0.301 - 0.082i$	$-0.303 - 0.120i$	$-0.247 - 0.115i$
	1P_1	$0.000 + 0.003i$	$-0.007 + 0.093i$	$0.004 + 0.099i$	$0.027 + 0.066i$	$0.041 + 0.029i$
	3P_1	$0.000 - 0.006i$	$0.026 - 0.228i$	$0.045 - 0.347i$	$0.043 - 0.345i$	$0.038 - 0.258i$
	1D_2	$0.000 + 0.000i$	$0.000 + 0.025i$	$-0.004 + 0.063i$	$-0.008 + 0.084i$	$-0.010 + 0.087i$
	3D_2	$0.000 + 0.000i$	$0.000 - 0.046i$	$-0.002 - 0.141i$	$0.004 - 0.246i$	$0.023 - 0.327i$
	1F_3	$0.000 + 0.000i$	$0.000 + 0.005i$	$0.000 + 0.023i$	$-0.002 + 0.042i$	$-0.007 + 0.058i$
	3F_3	$0.000 + 0.000i$	$0.000 - 0.008i$	$-0.001 - 0.040i$	$-0.003 - 0.089i$	$-0.006 - 0.145i$
	1G_4	$0.000 + 0.000i$	$0.000 + 0.001i$	$0.000 + 0.008i$	$0.000 + 0.019i$	$-0.001 + 0.031i$
	3G_4	$0.000 + 0.000i$	$0.000 - 0.001i$	$0.000 - 0.013i$	$-0.001 - 0.034i$	$-0.002 - 0.062i$
$p_{\text{lab}}(\text{MeV}/c)$	600	700	800	900	1000	
$\bar{p}p \rightarrow \bar{p}p$	1S_0	$-0.042 - 0.076i$	$-0.013 - 0.019i$	$0.036 + 0.007i$	$0.085 + 0.002i$	$0.123 - 0.026i$
	3P_0	$-0.162 - 0.024i$	$-0.236 + 0.098i$	$-0.245 + 0.207i$	$-0.213 + 0.294i$	$-0.159 + 0.356i$
	1P_1	$0.429 - 0.271i$	$0.289 - 0.330i$	$0.151 - 0.349i$	$0.027 - 0.331i$	$-0.075 - 0.280i$
	3P_1	$0.443 - 0.222i$	$0.360 - 0.167i$	$0.281 - 0.110i$	$0.215 - 0.056i$	$0.170 - 0.007i$
	1D_2	$0.721 + 0.032i$	$0.601 - 0.035i$	$0.482 - 0.110i$	$0.366 - 0.176i$	$0.253 - 0.223i$
	3D_2	$0.789 - 0.081i$	$0.714 - 0.090i$	$0.648 - 0.090i$	$0.585 - 0.077i$	$0.521 - 0.056i$
	1F_3	$0.971 + 0.077i$	$0.934 + 0.105i$	$0.874 + 0.126i$	$0.794 + 0.130i$	$0.703 + 0.112i$
	3F_3	$0.969 - 0.057i$	$0.944 - 0.055i$	$0.910 - 0.048i$	$0.870 - 0.041i$	$0.826 - 0.036i$
	1G_4	$0.998 + 0.030i$	$0.996 + 0.042i$	$0.992 + 0.058i$	$0.984 + 0.077i$	$0.969 + 0.101i$
	3G_4	$0.994 - 0.041i$	$0.990 - 0.048i$	$0.983 - 0.052i$	$0.974 - 0.051i$	$0.962 - 0.047i$
$\bar{p}p \rightarrow \bar{n}n$	1S_0	$-0.057 - 0.071i$	$-0.111 - 0.030i$	$-0.138 + 0.035i$	$-0.136 + 0.109i$	$-0.104 + 0.180i$
	3P_0	$-0.171 - 0.084i$	$-0.100 - 0.061i$	$-0.043 - 0.058i$	$-0.006 - 0.076i$	$0.008 - 0.106i$
	1P_1	$0.039 - 0.001i$	$0.027 - 0.019i$	$0.012 - 0.026i$	$-0.002 - 0.024i$	$-0.012 - 0.016i$
	3P_1	$0.039 - 0.125i$	$0.044 + 0.014i$	$0.063 + 0.127i$	$0.100 + 0.202i$	$0.149 + 0.242i$
	1D_2	$-0.009 + 0.078i$	$-0.007 + 0.065i$	$-0.007 + 0.054i$	$-0.009 + 0.045i$	$-0.011 + 0.040i$
	3D_2	$0.050 - 0.362i$	$0.073 - 0.348i$	$0.084 - 0.294i$	$0.082 - 0.213i$	$0.071 - 0.123i$
	1F_3	$-0.017 + 0.065i$	$-0.035 + 0.062i$	$-0.063 + 0.046i$	$-0.097 + 0.016i$	$-0.129 - 0.024i$
	3F_3	$-0.006 - 0.204i$	$-0.001 - 0.258i$	$0.012 - 0.303i$	$0.032 - 0.330i$	$0.056 - 0.337i$
	1G_4	$-0.001 + 0.041i$	$-0.003 + 0.048i$	$-0.005 + 0.052i$	$-0.008 + 0.053i$	$-0.015 + 0.053i$
	3G_4	$-0.004 - 0.095i$	$-0.006 - 0.129i$	$-0.007 - 0.163i$	$-0.007 - 0.197i$	$-0.004 - 0.230i$

TABLE VI. S -matrix elements of the coupled partial waves for $\bar{p}p \rightarrow \bar{p}p$.

$p_{\text{lab}}(\text{MeV}/c)$		100	200	300	400	500
${}^3S_1 - {}^3D_1$	S_{11}	$0.514 - 0.307i$	$0.207 - 0.290i$	$0.039 - 0.195i$	$-0.039 - 0.096i$	$-0.071 - 0.015i$
	S_{22}	$0.998 + 0.003i$	$0.974 + 0.015i$	$0.926 + 0.025i$	$0.865 + 0.034i$	$0.798 + 0.044i$
	S_{12}	$0.004 - 0.015i$	$-0.010 - 0.058i$	$-0.031 - 0.093i$	$-0.056 - 0.108i$	$-0.077 - 0.103i$
${}^3P_2 - {}^3F_2$	S_{11}	$0.971 + 0.021i$	$0.807 + 0.089i$	$0.558 + 0.111i$	$0.355 + 0.101i$	$0.220 + 0.095i$
	S_{22}	$1.000 + 0.000i$	$0.998 + 0.003i$	$0.991 + 0.008i$	$0.980 + 0.012i$	$0.964 + 0.018i$
	S_{12}	$0.000 - 0.003i$	$0.007 - 0.022i$	$0.016 - 0.038i$	$0.014 - 0.047i$	$0.004 - 0.055i$
${}^3D_3 - {}^3G_3$	S_{11}	$1.000 + 0.000i$	$0.998 + 0.010i$	$0.981 + 0.055i$	$0.919 + 0.146i$	$0.791 + 0.247i$
	S_{22}	$1.000 + 0.000i$	$1.000 + 0.000i$	$0.999 + 0.003i$	$0.996 + 0.007i$	$0.991 + 0.010i$
	S_{12}	$0.000 + 0.000i$	$0.000 - 0.005i$	$0.002 - 0.020i$	$0.008 - 0.037i$	$0.019 - 0.046i$
${}^3F_4 - {}^3H_4$	S_{11}	$1.000 + 0.000i$	$1.000 + 0.001i$	$1.000 + 0.005i$	$0.998 + 0.018i$	$0.990 + 0.045i$
	S_{22}	$1.000 + 0.000i$	$1.000 + 0.000i$	$1.000 + 0.001i$	$0.999 + 0.003i$	$0.998 + 0.005i$
	S_{12}	$0.000 + 0.000i$	$0.000 - 0.001i$	$0.000 - 0.007i$	$0.000 - 0.015i$	$0.002 - 0.026i$
$p_{\text{lab}}(\text{MeV}/c)$		600	700	800	900	1000
${}^3S_1 - {}^3D_1$	S_{11}	$-0.087 + 0.047i$	$-0.107 + 0.095i$	$-0.141 + 0.141i$	$-0.191 + 0.193i$	$-0.244 + 0.254i$
	S_{22}	$0.734 + 0.051i$	$0.671 + 0.047i$	$0.605 + 0.026i$	$0.526 - 0.016i$	$0.432 - 0.077i$
	S_{12}	$-0.092 - 0.078i$	$-0.097 - 0.040i$	$-0.095 - 0.001i$	$-0.089 + 0.027i$	$-0.082 + 0.037i$
${}^3P_2 - {}^3F_2$	S_{11}	$0.141 + 0.097i$	$0.097 + 0.103i$	$0.073 + 0.110i$	$0.059 + 0.116i$	$0.051 + 0.121i$
	S_{22}	$0.938 + 0.031i$	$0.892 + 0.048i$	$0.822 + 0.066i$	$0.725 + 0.074i$	$0.610 + 0.063i$
	S_{12}	$-0.009 - 0.060i$	$-0.024 - 0.058i$	$-0.042 - 0.050i$	$-0.062 - 0.038i$	$-0.085 - 0.027i$
${}^3D_3 - {}^3G_3$	S_{11}	$0.642 + 0.315i$	$0.518 + 0.354i$	$0.437 + 0.369i$	$0.401 + 0.357i$	$0.403 + 0.315i$
	S_{22}	$0.986 + 0.014i$	$0.981 + 0.021i$	$0.971 + 0.033i$	$0.952 + 0.055i$	$0.914 + 0.087i$
	S_{12}	$0.022 - 0.045i$	$0.014 - 0.041i$	$-0.003 - 0.037i$	$-0.026 - 0.032i$	$-0.055 - 0.023i$
${}^3F_4 - {}^3H_4$	S_{11}	$0.972 + 0.085i$	$0.940 + 0.132i$	$0.897 + 0.177i$	$0.855 + 0.211i$	$0.822 + 0.229i$
	S_{22}	$0.996 + 0.008i$	$0.994 + 0.012i$	$0.990 + 0.015i$	$0.987 + 0.019i$	$0.981 + 0.026i$
	S_{12}	$0.005 - 0.037i$	$0.009 - 0.046i$	$0.012 - 0.052i$	$0.013 - 0.056i$	$0.012 - 0.059i$

TABLE VII. S -matrix elements of the coupled partial waves for $\bar{p}p \rightarrow \bar{n}n$.

$p_{\text{lab}}(\text{MeV}/c)$		100	200	300	400	500
${}^3S_1 - {}^3D_1$	S_{11}	$-0.021 - 0.071i$	$-0.154 - 0.091i$	$-0.191 + 0.010i$	$-0.172 + 0.102i$	$-0.123 + 0.165i$
	S_{22}	$0.000 + 0.000i$	$-0.014 + 0.025i$	$-0.049 + 0.069i$	$-0.091 + 0.114i$	$-0.129 + 0.154i$
	S_{12}	$0.008 - 0.021i$	$0.003 - 0.148i$	$-0.042 - 0.228i$	$-0.098 - 0.269i$	$-0.146 - 0.280i$
	S_{21}	$0.000 + 0.000i$	$-0.012 - 0.093i$	$-0.055 - 0.179i$	$-0.108 - 0.229i$	$-0.154 - 0.248i$
${}^3P_2 - {}^3F_2$	S_{11}	$-0.001 + 0.000i$	$-0.077 + 0.013i$	$-0.162 - 0.026i$	$-0.181 - 0.058i$	$-0.170 - 0.053i$
	S_{22}	$0.000 + 0.000i$	$-0.001 + 0.003i$	$-0.005 + 0.015i$	$-0.011 + 0.032i$	$-0.016 + 0.050i$
	S_{12}	$0.000 + 0.000i$	$0.008 - 0.045i$	$0.027 - 0.099i$	$0.035 - 0.135i$	$0.026 - 0.162i$
	S_{21}	$0.000 + 0.000i$	$0.005 - 0.028i$	$0.019 - 0.073i$	$0.024 - 0.110i$	$0.015 - 0.141i$
${}^3D_3 - {}^3G_3$	S_{11}	$0.000 + 0.000i$	$-0.001 + 0.005i$	$-0.013 + 0.030i$	$-0.058 + 0.072i$	$-0.145 + 0.087i$
	S_{22}	$0.000 + 0.000i$	$0.000 + 0.000i$	$-0.001 + 0.004i$	$-0.003 + 0.012i$	$-0.006 + 0.021i$
	S_{12}	$0.000 + 0.000i$	$0.000 - 0.008i$	$0.002 - 0.037i$	$0.009 - 0.075i$	$0.023 - 0.107i$
	S_{21}	$0.000 + 0.000i$	$0.000 - 0.006i$	$0.001 - 0.029i$	$0.008 - 0.062i$	$0.021 - 0.092i$
${}^3F_4 - {}^3H_4$	S_{11}	$0.000 + 0.000i$	$0.000 + 0.001i$	$0.000 + 0.005i$	$-0.002 + 0.015i$	$-0.009 + 0.032i$
	S_{22}	$0.000 + 0.000i$	$0.000 + 0.000i$	$0.000 + 0.001i$	$0.000 + 0.004i$	$-0.001 + 0.010i$
	S_{12}	$0.000 + 0.000i$	$0.000 - 0.001i$	$0.000 - 0.012i$	$0.000 - 0.030i$	$0.002 - 0.052i$
	S_{21}	$0.000 + 0.000i$	$0.000 - 0.001i$	$0.000 - 0.009i$	$0.000 - 0.025i$	$0.002 - 0.045i$
$p_{\text{lab}}(\text{MeV}/c)$		600	700	800	900	1000
${}^3S_1 - {}^3D_1$	S_{11}	$-0.064 + 0.195i$	$-0.004 + 0.199i$	$0.050 + 0.180i$	$0.093 + 0.146i$	$0.120 + 0.105i$
	S_{22}	$-0.147 + 0.186i$	$-0.136 + 0.206i$	$-0.091 + 0.215i$	$-0.021 + 0.215i$	$0.059 + 0.207i$
	S_{12}	$-0.177 - 0.274i$	$-0.188 - 0.264i$	$-0.185 - 0.255i$	$-0.174 - 0.242i$	$-0.165 - 0.216i$
	S_{21}	$-0.183 - 0.251i$	$-0.193 - 0.247i$	$-0.189 - 0.244i$	$-0.177 - 0.235i$	$-0.166 - 0.211i$
${}^3P_2 - {}^3F_2$	S_{11}	$-0.152 - 0.030i$	$-0.129 - 0.003i$	$-0.102 + 0.018i$	$-0.073 + 0.032i$	$-0.045 + 0.038i$
	S_{22}	$-0.019 + 0.067i$	$-0.015 + 0.083i$	$0.001 + 0.097i$	$0.031 + 0.113i$	$0.073 + 0.136i$
	S_{12}	$0.007 - 0.185i$	$-0.020 - 0.204i$	$-0.048 - 0.214i$	$-0.074 - 0.213i$	$-0.096 - 0.195i$
	S_{21}	$-0.003 - 0.166i$	$-0.028 - 0.187i$	$-0.055 - 0.201i$	$-0.080 - 0.202i$	$-0.100 - 0.187i$
${}^3D_3 - {}^3G_3$	S_{11}	$-0.217 + 0.047i$	$-0.227 - 0.010i$	$-0.186 - 0.046i$	$-0.121 - 0.063i$	$-0.051 - 0.077i$
	S_{22}	$-0.009 + 0.031i$	$-0.011 + 0.043i$	$-0.014 + 0.056i$	$-0.020 + 0.073i$	$-0.035 + 0.089i$
	S_{12}	$0.034 - 0.128i$	$0.035 - 0.144i$	$0.026 - 0.160i$	$0.009 - 0.179i$	$-0.016 - 0.204i$
	S_{21}	$0.030 - 0.111i$	$0.029 - 0.128i$	$0.020 - 0.145i$	$0.002 - 0.165i$	$-0.022 - 0.190i$
${}^3F_4 - {}^3H_4$	S_{11}	$-0.025 + 0.054i$	$-0.053 + 0.073i$	$-0.086 + 0.082i$	$-0.110 + 0.078i$	$-0.115 + 0.068i$
	S_{22}	$-0.003 + 0.016i$	$-0.005 + 0.022i$	$-0.007 + 0.029i$	$-0.010 + 0.036i$	$-0.013 + 0.043i$
	S_{12}	$0.005 - 0.075i$	$0.010 - 0.097i$	$0.014 - 0.116i$	$0.016 - 0.134i$	$0.014 - 0.151i$
	S_{21}	$0.005 - 0.067i$	$0.009 - 0.088i$	$0.013 - 0.106i$	$0.014 - 0.123i$	$0.012 - 0.140i$

TABLE VIII. Phase-shift and inelasticity parameters of the uncoupled partial waves assuming isospin symmetry. δ is given in degrees.

$p_{\text{lab}}(\text{MeV}/c)$		100	200	300	400	500	600	700	800	900	1000
$^{11}S_0$	η	0.61	0.48	0.39	0.31	0.24	0.18	0.13	0.11	0.13	0.16
	δ	179.28	169.97	157.96	145.40	132.28	117.71	99.83	77.61	56.50	41.44
$^{31}S_0$	η	0.73	0.51	0.34	0.20	0.09	0.02	0.10	0.18	0.25	0.31
	δ	-14.44	-26.94	-38.41	-49.03	-57.58	-4.58	4.39	-3.48	-11.88	-20.11
$^{13}P_0$	η	0.82	0.50	0.39	0.36	0.35	0.35	0.34	0.33	0.31	0.29
	δ	179.87	168.27	148.53	139.70	113.53	99.67	87.73	77.52	68.97	62.10
$^{33}P_0$	η	0.99	0.95	0.81	0.55	0.25	0.05	0.21	0.33	0.43	0.49
	δ	-1.31	-4.79	-6.79	-6.48	-4.03	40.24	67.02	64.93	60.66	55.86
$^{11}P_1$	η	0.99	0.93	0.83	0.72	0.63	0.54	0.47	0.41	0.36	0.31
	δ	1.63	4.71	4.03	-0.24	-6.81	-14.75	-23.54	-32.88	-42.63	-52.76
$^{31}P_1$	η	0.99	0.93	0.81	0.68	0.56	0.48	0.41	0.35	0.31	0.27
	δ	-0.43	-1.43	-2.83	-5.73	-10.51	-16.86	-24.39	-32.75	-41.74	-51.22
$^{13}P_1$	η	1.00	0.99	0.96	0.89	0.76	0.59	0.43	0.34	0.35	0.40
	δ	-2.70	-10.23	-16.84	-20.52	-21.74	-17.29	-9.54	2.48	13.45	19.05
$^{33}P_1$	η	0.98	0.88	0.73	0.59	0.49	0.42	0.36	0.32	0.28	0.24
	δ	1.34	5.24	7.05	5.13	0.27	-6.53	-14.57	-23.42	-32.84	-42.76
$^{11}D_2$	η	1.00	1.00	0.98	0.93	0.84	0.73	0.60	0.48	0.38	0.31
	δ	0.13	1.42	3.34	4.89	5.42	4.40	1.51	-3.28	-9.93	-18.44
$^{31}D_2$	η	1.00	1.00	0.98	0.94	0.85	0.73	0.62	0.52	0.44	0.37
	δ	-0.04	-0.34	-0.52	-0.38	-0.47	-1.67	-4.53	-9.07	-15.06	-22.19
$^{13}D_2$	η	1.00	1.00	1.00	0.99	0.98	0.95	0.91	0.83	0.73	0.62
	δ	-0.20	-2.28	-5.76	-9.30	-12.17	-13.97	-14.52	-13.70	-11.56	-8.11
$^{33}D_2$	η	1.00	1.00	0.99	0.95	0.88	0.79	0.69	0.60	0.52	0.46
	δ	0.08	0.99	3.00	5.76	8.54	10.44	10.92	9.91	7.65	4.44
$^{11}F_3$	η	1.00	1.00	1.00	1.00	0.99	0.97	0.92	0.83	0.71	0.58
	δ	0.01	0.31	1.11	2.12	3.15	4.21	5.23	5.95	5.85	4.32
$^{31}F_3$	η	1.00	1.00	1.00	1.00	1.00	0.99	0.97	0.94	0.90	0.85
	δ	0.00	-0.10	-0.30	-0.41	-0.24	0.31	1.25	2.44	3.67	4.69
$^{13}F_3$	η	1.00	1.00	1.00	1.00	1.00	1.00	1.00	0.99	0.98	0.96
	δ	-0.01	-0.47	-1.85	-3.76	-5.78	-7.67	-9.28	-10.49	-11.25	-11.50
$^{33}F_3$	η	1.00	1.00	1.00	1.00	1.00	0.99	0.97	0.93	0.89	0.83
	δ	0.00	0.17	0.71	1.62	2.86	4.41	6.19	8.00	9.59	10.71
$^{11}G_4$	η	1.00	1.00	1.00	1.00	1.00	1.00	1.00	0.99	0.98	0.97
	δ	0.00	0.06	0.39	0.90	1.47	2.03	2.59	3.17	3.81	4.55
$^{31}G_4$	η	1.00	1.00	1.00	1.00	1.00	1.00	1.00	1.00	0.99	0.99
	δ	0.00	-0.02	-0.12	-0.26	-0.36	-0.36	-0.20	0.14	0.68	1.39
$^{13}G_4$	η	1.00	1.00	1.00	1.00	1.00	1.00	1.00	1.00	1.00	1.00
	δ	0.00	-0.09	-0.61	-1.53	-2.69	-3.92	-5.13	-6.26	-7.26	-8.10
$^{33}G_4$	η	1.00	1.00	1.00	1.00	1.00	1.00	1.00	1.00	0.99	0.98
	δ	0.00	0.03	0.21	0.56	1.05	1.66	2.42	3.30	4.33	5.45

TABLE IX. Phase-shift and inelasticity parameters of the coupled partial waves with $J = 1, 2$ assuming isospin symmetry. $\bar{\delta}$, $\bar{\epsilon}_J$ and ω_J are given in degrees.

$p_{\text{lab}}(\text{MeV}/c)$		100	200	300	400	500	600	700	800	900	1000
$^{13}S_1$	η_S	0.63	0.37	0.22	0.15	0.14	0.14	0.16	0.17	0.19	0.22
	$\bar{\delta}_S$	160.16	141.90	125.45	111.64	99.16	86.70	76.21	69.19	65.54	64.21
	ω_1	3.71	9.61	15.24	20.32	24.93	29.08	31.90	33.49	34.89	37.29
	—										
	$\bar{\epsilon}_1$	1.62	6.90	12.60	17.51	20.74	21.16	19.42	16.88	14.46	12.61
	η_D	1.00	1.00	0.99	0.98	0.96	0.92	0.88	0.84	0.79	0.74
$^{13}D_1$	$\bar{\delta}_D$	0.17	2.01	5.83	11.08	16.81	21.13	22.53	21.15	17.91	13.54
	η_S	0.63	0.43	0.32	0.25	0.20	0.17	0.14	0.12	0.13	0.18
	$\bar{\delta}_S$	173.41	166.53	159.57	152.23	144.07	134.41	121.85	104.94	87.16	76.85
	ω_1	-0.91	-1.57	-1.60	-1.83	-3.08	-6.20	-12.04	-20.87	-30.83	-41.24
	—										
	$\bar{\epsilon}_1$	-0.71	-2.87	-5.09	-7.00	-8.64	-10.00	-10.48	-8.07	-1.29	4.78
$^{33}D_1$	η_D	1.00	1.00	1.00	0.99	0.97	0.94	0.89	0.83	0.76	0.69
	$\bar{\delta}_D$	-0.03	-0.49	-1.42	-2.43	-3.20	-3.60	-3.79	-5.09	-10.94	-21.33
	η_P	0.96	0.74	0.42	0.21	0.10	0.07	0.06	0.06	0.05	0.04
	$\bar{\delta}_P$	0.70	3.82	6.18	7.70	14.21	27.68	35.57	37.95	41.92	51.99
	ω_2	-0.76	-2.19	-2.36	-1.09	2.34	8.38	13.50	17.31	20.64	22.71
	—										
$^{13}F_2$	$\bar{\epsilon}_2$	-0.18	-2.11	-5.30	-8.55	-11.14	-11.37	-9.80	-7.77	-3.92	3.71
	η_F	1.00	1.00	1.00	1.00	1.00	0.99	0.97	0.94	0.89	0.84
	$\bar{\delta}_F$	0.01	0.23	0.82	1.44	1.68	1.49	2.06	3.35	5.59	9.60
	η_P	0.99	0.91	0.75	0.57	0.42	0.32	0.26	0.21	0.17	0.15
	$\bar{\delta}_P$	0.38	2.34	5.48	8.41	10.48	11.72	12.32	12.79	14.08	17.35
	ω_2	0.28	0.85	1.01	0.65	-0.11	-1.18	-2.49	-3.96	-5.49	-6.91
$^{33}F_2$	—										
	$\bar{\epsilon}_2$	0.06	0.67	1.74	2.89	4.01	5.19	6.58	8.31	10.38	12.49
	η_F	1.00	1.00	1.00	1.00	0.99	0.97	0.93	0.85	0.73	0.58
	$\bar{\delta}_F$	0.00	-0.06	-0.29	-0.64	-1.00	-1.26	-1.40	-1.63	-2.48	-5.12

TABLE X. Phase-shift and inelasticity parameters of the coupled partial waves with $J = 3, 4$ assuming isospin symmetry. $\bar{\delta}$, $\bar{\epsilon}_J$ and ω_J are given in degrees.

$p_{\text{lab}}(\text{MeV}/c)$		100	200	300	400	500	600	700	800	900	1000
$^{13}D_3$	η_D	1.00	1.00	0.97	0.89	0.74	0.58	0.47	0.42	0.41	0.41
	$\bar{\delta}_D$	0.02	0.47	2.52	7.07	13.52	19.85	24.11	24.78	21.37	14.52
	ω_3	-0.24	-1.04	-1.71	-1.68	-0.63	1.37	4.05	7.18	10.92	15.92
	—										
	$\bar{\epsilon}_3$	-0.01	-0.41	-1.59	-3.29	-5.03	-6.37	-7.10	-7.34	-7.44	-7.86
	η_G	1.00	1.00	1.00	1.00	1.00	1.00	1.00	0.99	0.99	0.96
$^{13}G_3$	$\bar{\delta}_G$	0.00	0.03	0.23	0.57	0.94	1.26	1.61	2.16	3.07	4.40
$^{33}D_3$	η_D	1.00	1.00	1.00	0.99	0.96	0.91	0.84	0.76	0.68	0.61
	$\bar{\delta}_D$	0.00	0.08	0.56	1.97	4.68	8.61	13.05	16.96	19.53	20.49
	ω_3	0.10	0.42	0.71	0.79	0.57	0.01	-0.85	-1.96	-3.23	-4.57
	—										
	$\bar{\epsilon}_3$	0.00	0.14	0.51	1.05	1.67	2.33	3.04	3.86	4.92	6.38
	η_G	1.00	1.00	1.00	1.00	1.00	1.00	1.00	0.99	0.99	0.97
$^{33}G_3$	$\bar{\delta}_G$	0.00	-0.01	-0.07	-0.20	-0.37	-0.56	-0.71	-0.79	-0.71	-0.35
$^{13}F_4$	η_F	1.00	1.00	1.00	1.00	0.99	0.96	0.92	0.87	0.82	0.79
	$\bar{\delta}_F$	0.00	0.04	0.29	0.96	2.25	4.16	6.50	8.79	10.48	11.18
	ω_4	-0.10	-0.45	-0.93	-1.23	-1.20	-0.76	0.15	1.59	3.63	6.36
	—										
	$\bar{\epsilon}_4$	0.00	-0.08	-0.52	-1.26	-2.19	-3.19	-4.18	-5.10	-5.91	-6.64
	η_H	1.00	1.00	1.00	1.00	1.00	1.00	1.00	1.00	1.00	1.00
$^{13}H_4$	$\bar{\delta}_H$	0.00	0.00	0.06	0.21	0.43	0.70	0.99	1.27	1.57	1.88
$^{33}F_4$	η_F	1.00	1.00	1.00	1.00	1.00	1.00	1.00	0.99	0.98	0.95
	$\bar{\delta}_F$	0.00	0.00	-0.01	0.05	0.29	0.80	1.62	2.69	3.86	4.86
	ω_4	-0.93	-2.63	-3.95	-4.78	-5.30	-5.65	-5.91	-6.14	-6.36	-6.57
	—										
	$\bar{\epsilon}_4$	0.00	0.03	0.17	0.41	0.72	1.05	1.41	1.77	2.15	2.56
	η_H	1.00	1.00	1.00	1.00	1.00	1.00	1.00	1.00	1.00	1.00
$^{33}H_4$	$\bar{\delta}_H$	0.00	0.00	-0.02	-0.07	-0.15	-0.25	-0.36	-0.46	-0.54	-0.59

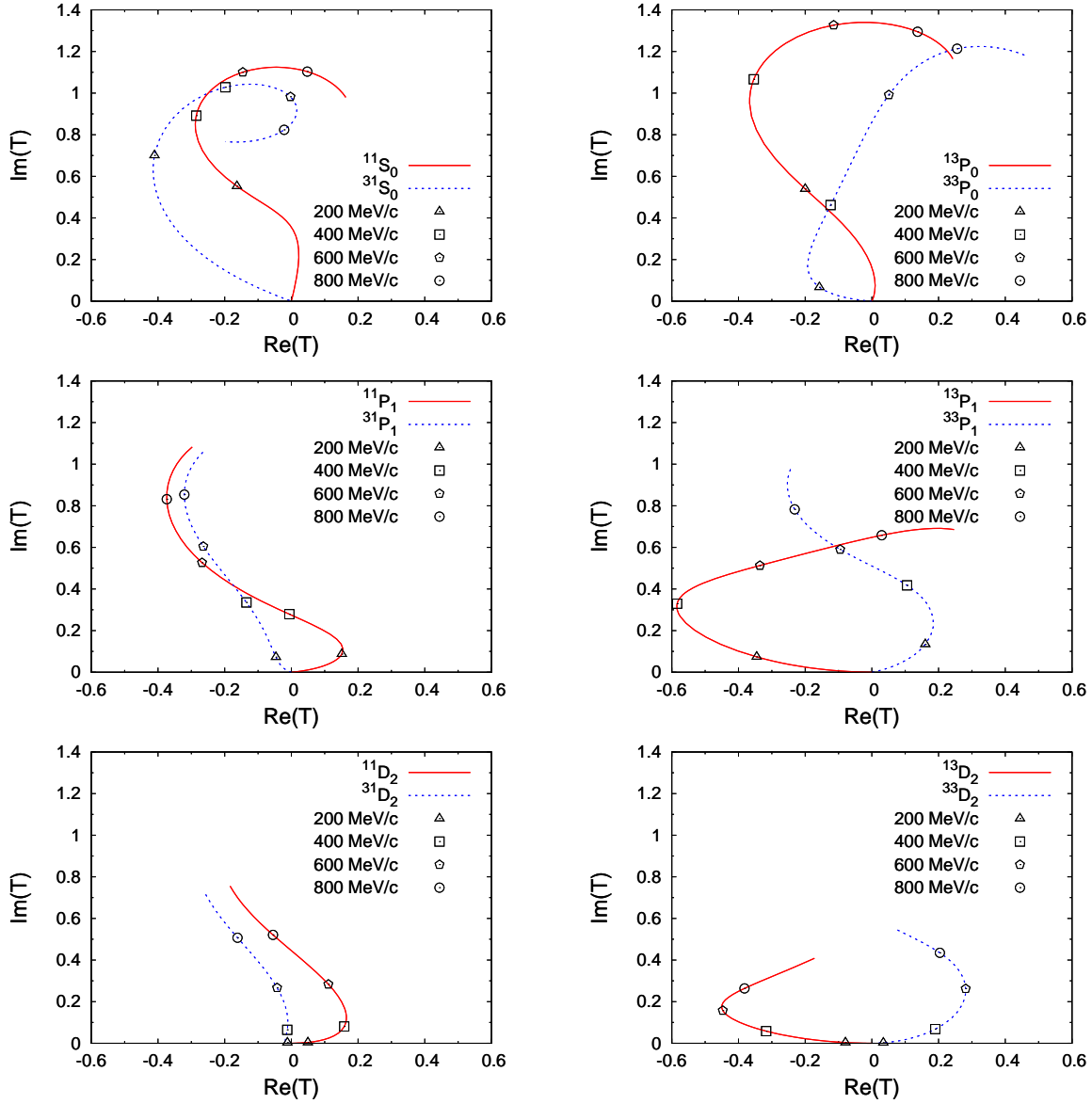


FIG. 15. (Color online) The Argand diagrams for the uncoupled S , P , and D waves, assuming isospin symmetry. The symbols on the lines denote the values of the antiproton laboratory momenta.

VIII. SUMMARY

In summary, motivated by renewed experimental interest in low-energy antiproton-proton scattering, we have presented a new energy-dependent PWA of all $\bar{p}p$ scattering data below 925 MeV/c antiproton laboratory momentum. We have improved the model independence and quality of the PWA by using for the long-range interaction, next to the electromag-

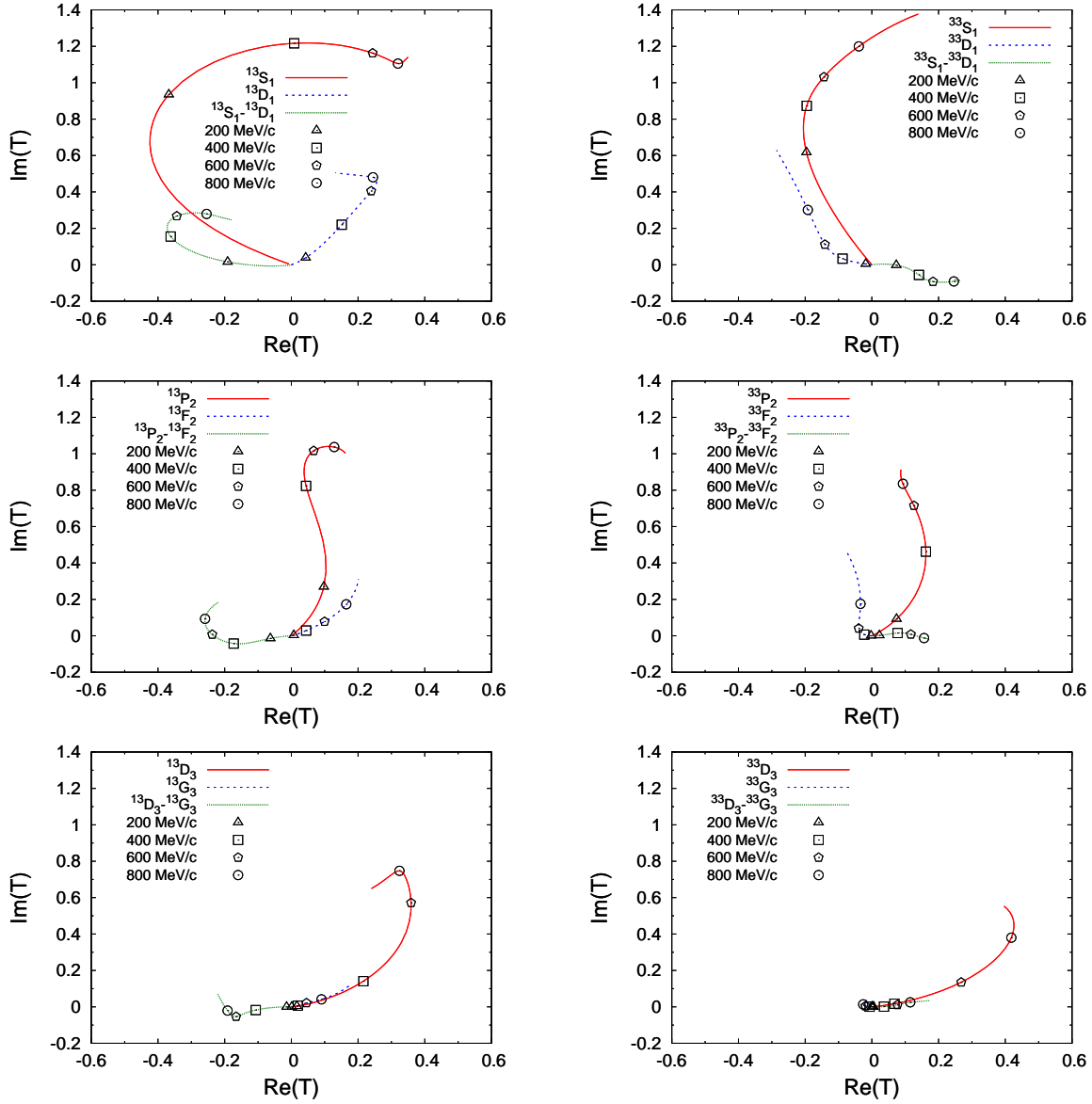


FIG. 16. (Color online) The Argand diagrams for the coupled S - D , P - F , and D - G waves, assuming isospin symmetry. The symbols on the lines denote the values of the antiproton laboratory momenta.

netic potential, the charge-conjugated one- and two-pion exchange potential derived from the effective chiral Lagrangian of QCD. We have updated the database and included the high-quality differential cross sections and analyzing powers for charge-exchange scattering $\bar{p}p \rightarrow \bar{n}n$ that were measured in the last years of operation of LEAR. The final database contains 3749 scattering data, which are fitted with an excellent $\chi^2_{\min}/N_{\text{dat}} = 1.000$ or $\chi^2_{\min}/N_{\text{df}} = 1.048$. This implies that the long-range potential provides an excellent descrip-

tion of $\bar{p}p$ elastic and charge-exchange scattering, which we count as a success for chiral effective field theory. Further improvement of the PWA is certainly possible, but it will require additional high-quality experimental data. Below 400 MeV/ c , there are hardly scattering data available. Spin observables will further constrain the PWA solution, provided they are precise enough. The results presented in this paper will serve as the starting point for more specific investigations of low-energy antiproton-proton scattering.

ACKNOWLEDGEMENTS

We would like to thank our colleagues at KVI for useful discussions. D. Zhou would like to thank F. Jin for help with the figures and W. Kruithof for help with the tables.

APPENDIX

In this Appendix, we study in more detail the statistical quality of the final antiproton-proton database, by investigating the distribution of the contributions of the $N_{\text{dat}} = 3749$ individual data points to the total χ^2 , χ_{tot}^2 [25]. In the PWA, this distribution is given by

$$P_{1,\text{analysis}}(\chi^2) = \frac{1}{N_{\text{dat}}} \sum_{i=1}^{N_{\text{dat}}} \delta(\chi^2 - \chi_i^2) . \quad (44)$$

In Fig. 17 we plot this distribution as a histogram and compare it to the theoretical χ^2 distribution for 1 degree of freedom,

$$P_1(\chi^2) = \frac{1}{\sqrt{2\pi}} t^{-1/2} e^{-t/2} . \quad (45)$$

In order to make this comparison quantitative, we give the moments, the central moments, and the corresponding errors for the distributions. For a distribution $P(t)$, with $t \geq 0$, we define the moments μ'_n and the central moments μ_n by

$$\begin{aligned} \mu'_n &= \int_0^\infty dt P(t) t^n , \\ \mu_n &= \int_0^\infty dt P(t) (t - \mu'_1)^n , \end{aligned} \quad (46)$$

respectively. The errors on the moments are given by

$$\sigma_{\mu'_n} = \left[\frac{\mu'_{2n} - (\mu'_n)^2}{N_{\text{dat}}} \right]^{1/2} , \quad (47)$$

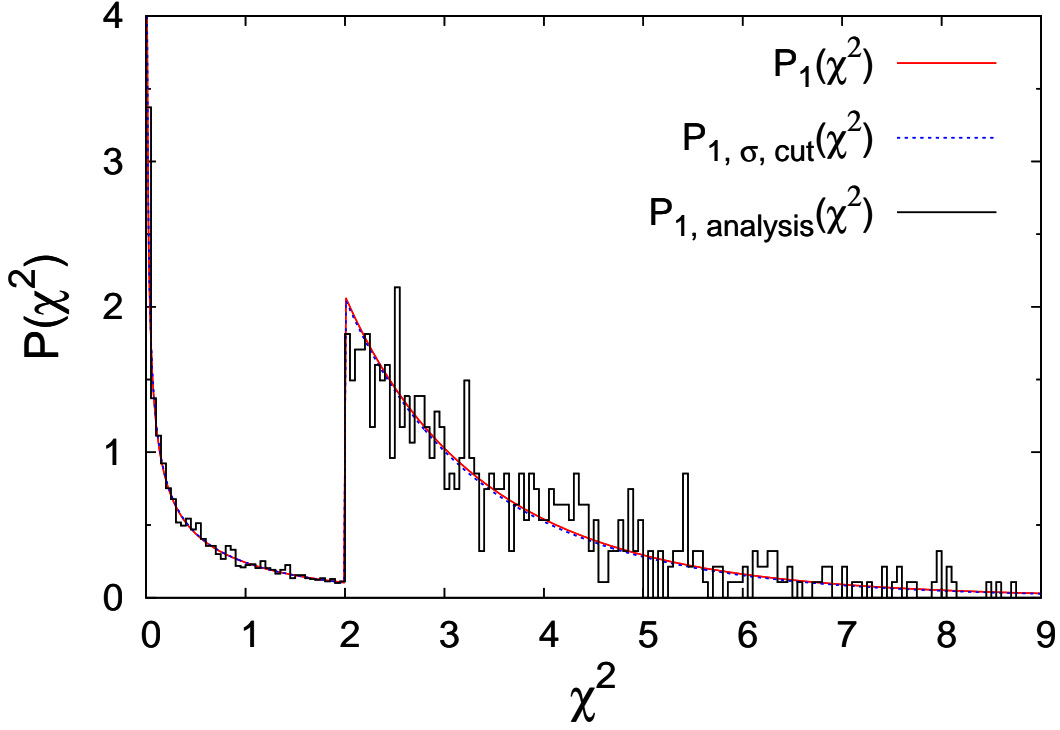


FIG. 17. (Color online) Probability distribution functions versus χ^2 . The tails, with the values $\chi^2 > 2$, are enlarged by a factor of 20. The histogram contains 3749 data points in bins with $\Delta\chi^2 = 0.05$.

and similarly for σ_{μ_n} . The lowest moments and their errors are given in Table XI. The agreement between the moments of $P_1(\chi^2)$ and $P_{1,\text{analysis}}(\chi^2)$ is reasonable, but not perfect.

In fact, for two reasons $P_1(\chi^2)$ is not the best distribution to compare to. First, while the first moment of $P_1(\chi^2)$ is $\mu'_1 = 1$, that of $P_{1,\text{analysis}}(\chi^2)$ is $\mu'_1 = \chi_{\text{tot}}^2/N_{\text{dat}}$. Since $\langle\chi_{\text{tot}}^2\rangle = N_{\text{df}}$, we should compare to a narrower distribution $P(\chi^2) = \beta^{-1}P_1(\beta^{-1}\chi^2)$ with $\beta = N_{\text{df}}/N_{\text{dat}}$. Second, the data points with individual $\chi_i^2 > 9$ were rejected, which affects the tail of the distribution and the higher moments. Therefore, it is better to compare $P_{1,\text{analysis}}(\chi^2)$ to

$$P_{1,\sigma,\text{cut}}(\chi^2) = \left[\sigma\sqrt{2}\gamma\left(\frac{1}{2}, \frac{9}{2}\sigma^{-2}\right) \right]^{-1} (\chi^2)^{-1/2} e^{-\chi^2/2\sigma^2} \theta(9 - \chi^2), \quad (48)$$

where $\gamma(s, z) = \int_0^z t^{s-1} e^{-t} dt$ is the lower incomplete gamma function and σ is a constant chosen to satisfy $\langle\chi^2\rangle = N_{\text{df}}/N_{\text{dat}}$; in our case, $N_{\text{df}} = 3578$ and $N_{\text{dat}} = 3749$, therefore we have $\sigma = 0.989$ and $\gamma(\frac{1}{2}, \frac{9}{2\sigma^2}) = 1.768$. The Heaviside step function $\theta(9 - \chi^2)$ removes the tail with $\chi^2 > 9$. $P_{1,\sigma,\text{cut}}(\chi^2)$ is also plotted in Fig. 17 and its lowest moments with errors

TABLE XI. Moments μ'_n and central moments μ_n of the database of the PWA and of the two theoretical probability distribution functions. The errors are given for $N_{\text{dat}} = 3749$, where the contributions of the normalization data are included.

	$P_1(\chi^2)$	$P_{1,\sigma,\text{cut}}(\chi^2)$	$P_{1,\text{analysis}}(\chi^2)$
μ'_1	1.00 ± 0.02	0.95 ± 0.02	1.00 ± 0.02
μ'_2	3.00 ± 0.16	2.59 ± 0.11	2.80 ± 0.12
μ'_3	15.0 ± 1.6	10.7 ± 0.7	11.8 ± 0.8
μ'_4	105 ± 23	56 ± 5	62 ± 6
μ_2	2.00 ± 0.12	1.67 ± 0.08	1.80 ± 0.08
μ_3	8.0 ± 1.3	5.1 ± 0.5	5.4 ± 0.5
μ_4	60 ± 18	26.8 ± 3.1	28.5 ± 3.1

are given in Table XI as well. The agreement between the moments of $P_{1,\text{analysis}}(\chi^2)$ and $P_{1,\sigma,\text{cut}}(\chi^2)$ is good, which implies that the χ^2 distribution of the PWA is close to what is expected for statistical data.

-
- [1] The PAX collaboration, www2.fz-juelich.de/ikp/pax.
 - [2] J.S. Ball and G.F. Chew, Phys. Rev. **109**, 1385 (1958); J.S. Ball and J.R. Fulco, Phys. Rev. **113**, 647 (1959).
 - [3] M.S. Spergel, Il Nuovo Cimento A **47**, 410 (1967).
 - [4] O.D. Dalkarov and F. Myhrer, Il Nuovo Cimento **40A**, 152 (1977).
 - [5] R.J.N. Phillips, Rev. Mod. Phys. **39**, 681 (1967).
 - [6] R.A. Bryan and R.J.N. Phillips, Nucl. Phys. **B5**, 201 (1968); *ibid.* **B7**, 481(E) (1968).
 - [7] F. Myhrer and A. Gersten, Il Nuovo Cimento **37A**, 21 (1977).
 - [8] C.B. Dover and J.-M. Richard, Phys. Rev. C **21**, 1466 (1980); *ibid.* **25**, 1952 (1982).
 - [9] M. Kohno and W. Weise, Nucl. Phys. **A454**, 429 (1986).
 - [10] T. Hippchen, K. Holinde, and W. Plessas, Phys. Rev. C **39**, 761 (1989).
 - [11] T. Hippchen, J. Haidenbauer, K. Holinde, and V. Mull, Phys. Rev. C **44**, 1323 (1991).
 - [12] V. Mull and K. Holinde, Phys. Rev. C **51**, 2360 (1995).
 - [13] J. Côté, M. Lacombe, B. Loiseau, B. Moussallam, and R. Vinh Mau, Phys. Rev. Lett. **48**, 1319 (1982).

- [14] M. Lacombe, B. Loiseau, B. Moussallam, and R. Vinh Mau, Phys. Rev. C **29**, 1800 (1984).
- [15] M. Pignone, M. Lacombe, B. Loiseau, and R. Vinh Mau, Phys. Rev. Lett. **67**, 2423 (1991).
- [16] M. Pignone, M. Lacombe, B. Loiseau, and R. Vinh Mau, Phys. Rev. C **50**, 2710 (1994).
- [17] B. El-Bennich, M. Lacombe, B. Loiseau, and R. Vinh Mau, Phys. Rev. C **59**, 2313 (1999).
- [18] B. El-Bennich, M. Lacombe, B. Loiseau, and S. Wycech, Phys. Rev. C **79**, 054001 (2009).
- [19] P.H. Timmers, W.A. van der Sanden, and J.J. de Swart, Phys. Rev. D **29**, 1928 (1984).
- [20] P.H. Timmers, W.A. van der Sanden, and J.J. de Swart, Phys. Rev. D **31**, 99 (1985).
- [21] G.Q. Liu and F. Tabakin, Phys. Rev. C **41**, 665 (1990).
- [22] R.G.E. Timmermans, Th.A. Rijken, and J.J. de Swart, Phys. Rev. Lett. **67**, 1074 (1991).
- [23] R. Timmermans, Th.A. Rijken, and J.J. de Swart, Phys. Rev. C **50**, 48 (1994).
- [24] R. Timmermans, Th.A. Rijken, and J.J. de Swart, Phys. Rev. C **52**, 1145 (1995).
- [25] J.R. Bergervoet, P.C. van Campen, W.A. van der Sanden, and J.J. de Swart, Phys. Rev. C **38**, 15 (1988).
- [26] J.R. Bergervoet, P.C. van Campen, R.A.M. Klomp, J.-L. de Kok, T.A. Rijken, V.G.J. Stoks, and J.J. de Swart, Phys. Rev. C **41**, 1435 (1990).
- [27] V.G.J. Stoks, R.A.M. Klomp, M.C.M. Rentmeester, and J.J. de Swart, Phys. Rev. C **48**, 792 (1993).
- [28] M.C.M. Rentmeester, R.G.E. Timmermans, J.L. Friar, and J.J. de Swart, Phys. Rev. Lett. **82**, 4992 (1999).
- [29] M.C.M. Rentmeester, R.G.E. Timmermans, and J.J. de Swart, Phys. Rev. C **67**, 044001 (2003).
- [30] M.M. Nagels, T.A. Rijken, and J.J. de Swart, Phys. Rev. D **17**, 768 (1978).
- [31] V.G.J. Stoks, R.A.M. Klomp, C.P.F. Terheggen, and J.J. de Swart, Phys. Rev. C **49**, 2950 (1994).
- [32] V.G.J. Stoks and J.J. de Swart, Phys. Rev. C **42**, 1235 (1990).
- [33] P. LaFrance, F. Lehar, B. Loiseau, and P. Winternitz, Helv. Phys. Acta **65**, 611 (1992).
- [34] R.L. Jaffe and F.E. Low, Phys. Rev. D **19**, 2105 (1979); R.L. Jaffe, in *Asymptotic Realms of Physics*, edited by A.H. Guth, K. Huang, and R.L. Jaffe (The MIT Press, 1983), p. 100.
- [35] B.L.G. Bakker and P.J. Mulders, Adv. Nucl. Phys. **17**, 1 (1986).
- [36] G.J.M. Austen and J.J. de Swart, Phys. Rev. Lett. **50**, 2039 (1983).
- [37] C. Ordóñez and U. van Kolck, Phys. Lett. B **291**, 459 (1992).

- [38] N. Kaiser, R. Brockmann, and W. Weise, Nucl. Phys. **A625**, 758 (1997).
- [39] V. Stoks, R. Timmermans, and J.J. de Swart, Phys. Rev. C **47**, 512 (1993).
- [40] J.J. de Swart, M.C.M. Rentmeester, and R.G.E. Timmermans, Pion-Nucleon Newsletter **13**, 96 (1997).
- [41] R.G.E. Timmermans, T.A. Rijken, and J.J. de Swart, Nucl. Phys. **A479**, 383c (1988).
- [42] J.J. de Swart, T.A. Rijken, P.M. Maessen, and R. Timmermans, Il Nuovo Cimento **102A**, 203 (1989).
- [43] R.G.E. Timmermans, Th.A. Rijken, and J.J. de Swart, Phys. Lett. B **257**, 227 (1991).
- [44] R.G.E. Timmermans, Th.A. Rijken, and J.J. de Swart, Phys. Rev. D **45**, 2288 (1992).
- [45] R.P. Hamilton, T.P. Pun, R.D. Tripp, H. Nicholson, D.M. Lazarus, Phys. Rev. Lett. **44**, 1179 (1980).
- [46] W. Brückner, B. Cujec, H. Döbbeling, K. Dworschak, F. Güttner, H. Kneis, S. Majewski, M. Nomachi, S. Paul, B. Povh, R.D. Ransome, T.-A. Shibata, M. Treichel, and Th. Walcher, Zeit. Phys. **A335**, 217 (1990).
- [47] W. Brückner, H. Döbbeling, F. Güttner, D. von Harrach, H. Kneis, S. Majewski, M. Nomachi, S. Paul, B. Povh, R.D. Ransome, T.-A. Shibata, M. Treichel, and Th. Walcher, Phys. Lett. **166B**, 113 (1986).
- [48] W. Brückner, B. Cujec, H. Döbbeling, K. Dworschak, H. Kneis, S. Majewski, M. Nomachi, S. Paul, B. Povh, R.D. Ransome, T.-A. Shibata, M. Treichel, and Th. Walcher, Zeit. Phys. **A339**, 367 (1991).
- [49] W. Brückner, H. Döbbeling, F. Güttner, D. von Harrach, H. Kneis, S. Majewski, M. Nomachi, S. Paul, B. Povh, R.D. Ransome, T.-A. Shibata, M. Treichel, and Th. Walcher, Phys. Lett. **169B**, 302 (1986).
- [50] D. Spencer and D.N. Edwards, Nucl. Phys. **B19**, 501 (1970).
- [51] W. Brückner, B. Cujec, H. Döbbeling, K. Dworschak, F. Güttner, H. Kneis, S. Majewski, M. Nomachi, S. Paul, B. Povh, R.D. Ransome, T.-A. Shibata, M. Treichel, and Th. Walcher, Phys. Lett. B **197**, 463 (1987); *ibid.* **199**, 596(E) (1987).
- [52] D.V. Bugg, J. Hall, A.S. Clough, R.L. Shypit, K. Bos, J.C. Kluyver, R.A. Kunne, L. Linssen, R. Birsa, F. Bradamante, S. Dalla Torre-Colautti, A. Martin, A. Penzo, P. Schiavon, A. Villari, E. Heer, C. LeLuc, Y. Onel, and D. Rapin, Phys. Lett. B **194**, 563 (1987).
- [53] L. Linssen, C.I. Beard, R. Birsa, K. Bos, F. Bradamante, D.V. Bugg, A.S. Clough, S. Dalla

- Torre-Colautti, M. Giorgi, J.R. Hall, J.C. Kluyver, R.A. Kunne, C. Lechanoine-LeLuc, A. Martin, Y. Onel, A. Penzo, D. Rapin, P. Schiavon, R.L. Shypit, and A. Villari, Nucl. Phys. **A469**, 726 (1987).
- [54] M. Alston-Garnjost, R. Kenney, D. Pollard, R. Ross, R. Tripp, and H. Nicholson, Phys. Rev. Lett. **35**, 1685 (1975).
- [55] B. Conforto, G. Fidecaro, H. Steiner, R. Bizzarri, P. Guidoni, F. Marcelja, G. Brautti, E. Castelli, M. Ceschia, and M. Sessa, Il Nuovo Cimento A **54**, 441 (1968).
- [56] M. Cresti, L. Peruzzo, and G. Sartori, Phys. Lett. **132B**, 209 (1983).
- [57] R.P. Hamilton, T.P. Pun, R.D. Tripp, D.M. Lazarus, and H. Nicholson, Phys. Rev. Lett. **44**, 1182 (1980).
- [58] V. Ashford, M.E. Sainio, M. Sakitt, and J. Skelly, Phys. Rev. Lett. **54**, 518 (1985).
- [59] S. Sakamoto, T. Hashimoto, F. Sai, and S.S. Yamamoto, Nucl. Phys. **B195**, 1 (1982).
- [60] A.S. Clough, C.I. Beard, D.V. Bugg, J.A. Edgington, J. Hall, K. Bos, J.C. Kluyver, R.A. Kunne, L. Linssen, R. Birsa, F. Bradamante, S. Dalla Torre-Colautti, M. Giorgi, A. Martin, A. Penzo, P. Schiavon, A. Villari, S. Degli-Agosti, E. Heer, R. Hess, C. Lechanoine-LeLuc, Y. Onel, and D. Rapin, Phys. Lett. **146B**, 299 (1984).
- [61] T. Kageyama, T. Fujii, K. Nakamura, F. Sai, S. Sakamoto, S. Sato, T. Takahashi, T. Tanimori, S.S. Yamamoto, and Y. Takada, Phys. Rev. D **35**, 2655 (1987).
- [62] K. Nakamura, T. Fujii, T. Kageyama, F. Sai, S. Sakamoto, S. Sato, T. Takahashi, T. Tanimori, and S.S. Yamamoto, Phys. Rev. Lett. **53**, 885 (1984).
- [63] T. Kamae, H. Aihara, J. Chiba, H. Fujii, T. Fujii, H. Iwasaki, K. Nakamura, T. Sumiyoshi, Y. Takada, T. Takeda, M. Yamauchi, H. Fukuma, and T. Takeshita, Phys. Rev. Lett. **44**, 1439 (1980).
- [64] K. Nakamura, H. Aihara, J. Chiba, H. Fujii, T. Fujii, H. Iwasaki, T. Kamae, T. Sumiyoshi, Y. Takada, T. Takeda, M. Yamauchi, H. Fukuma, and T. Takeshita, Phys. Rev. D **29**, 349 (1984).
- [65] M. Alston-Garnjost, R.P. Hamilton, R.W. Kenney, D.L. Pollard, R.D. Tripp, H. Nicholson, and D.M. Lazarus, Phys. Rev. Lett. **43**, 1901 (1979).
- [66] H. Iwasaki, H. Aihara, J. Chiba, H. Fujii, T. Fujii, T. Kamae, K. Nakamura, T. Sumiyoshi, Y. Takada, T. Takeda, M. Yamauchi, and H. Fukuma, Phys. Lett. **103B**, 247 (1981).
- [67] R. Bizzarri, B. Conforto, G.C. Gialanella, P. Guidoni, F. Marcelja, E. Castelli, M. Ceschia,

- and M. Sessa, *Il Nuovo Cimento A* **54**, 456 (1968).
- [68] F. Perrot-Kunne, R. Bertini, M. Costa, H. Catz, A. Chaumeaux, J.-C. Faivre, E. Vercellin, J. Arvieux, J. Yonnet, B. van den Brandt, D.R. Gill, J.A. Konter, S. Mango, G.D. Wait, E. Boschitz, W. Gyles, W. List, C. Otterman, R. Tacik, and M. Wessler, *Phys. Lett. B* **261**, 188 (1991).
 - [69] T. Tsuboyama, Y. Kubota, F. Sai, S. Sakamoto, and S.S. Yamamoto, *Phys. Rev. D* **28**, 2135 (1983).
 - [70] R.A. Kunne, C.I. Beard, R. Birsa, K. Bos, F. Bradamante, D.V. Bugg, A.S. Clough, S. Dalla Torre-Colautti, S. Degli-Agosti, J.A. Edgington, J.R. Hall, E. Heer, R. Hess, J.C. Kluyver, C. Lechanoine-LeLuc, L. Linssen, A. Martin, T.O. Niinikoski, Y. Onel, A. Penzo, D. Rapin, J.M. Rieubland, A. Rijllart, P. Schiavon, R.L. Shypit, F. Tassarotto, A. Villari, and P. Wells, *Phys. Lett. B* **206**, 557 (1988).
 - [71] R.A. Kunne, C.I. Beard, R. Birsa, K. Bos, F. Bradamante, D.V. Bugg, A.S. Clough, S. Dalla Torre-Colautti, J.A. Edgington, J.R. Hall, E. Heer, R. Hess, J.C. Kluyver, C. Lechanoine-LeLuc, L. Linssen, A. Martin, T.O. Niinikoski, Y. Onel, A. Penzo, D. Rapin, J.M. Rieubland, A. Rijllart, P. Schiavon, R.L. Shypit, F. Tassarotto, A. Villari, and P. Wells, *Nucl. Phys. B* **323**, 1 (1989).
 - [72] A. Ahmidouch, E. Heer, R. Hess, C. Lechanoine-Leluc, Ch. Mascarini, D. Rapin, R. Birsa, F. Bradamante, A. Bressan, S. Dalla Torre-Colautti, M. Giorgi, M. Lamanna, A. Martin, A. Penzo, P. Schiavon, F. Tassarotto, M.P. Macciotta, A. Masoni, G. Puddu, S. Serchi, J. Arvieux, R. Bertini, R.A. Kunne, H. Catz, J.C. Faivre, F. Perrot-Kunne, M. Agnello, F. Iazzi, B. Minetti, T. Bressani, E. Chiavassa, N. De Marco, A. Musso, and A. Piccotti, *Phys. Lett. B* **364**, 116 (1995).
 - [73] R. Birsa, F. Bradamante, A. Bressan, S. Dalla Torre-Colautti, M. Giorgi, M. Lamanna, A. Martin, A. Penzo, P. Schiavon, F. Tassarotto, M.P. Macciotta, A. Masoni, G. Puddu, S. Serchi, T. Niinikoski, A. Rijllart, A. Ahmidouch, E. Heer, R. Hess, C. Lechanoine-LeLuc, C. Mascarini, D. Rapin, J. Arvieux, R. Bertini, H. Catz, J.C. Faivre, R.A. Kunne, F. Perrot-Kunne, M. Agnello, F. Iazzi, B. Minetti, T. Bressani, E. Chiavassa, N. De Marco, A. Musso, and A. Piccotti, *Phys. Lett. B* **273**, 533 (1991).
 - [74] A. Ahmidouch, E. Heer, R. Hess, C. Lechanoine-Leluc, C. Mascarini, D. Rapin, R. Birsa, F. Bradamante, A. Bressan, S. Dalla Torre-Colautti, M. Giorgi, M. Lamanna, A. Martin,

- A. Penzo, P. Schiavon, F. Tassarotto, M.P. Macciotta, A. Masoni, G. Puddu, S. Serici, T. Niinikoski, A. Rijllart, H. Catz, J.C. Faivre, F. Perrot-Kunne, J. Arvieux, R. Bertini, R.A. Kunne, M. Agnello, F. Iazzi, B. Minetti, T. Bressani, E. Chiavassa, N. De Marco, A. Musso, and A. Piccotti, Nucl. Phys. **B444**, 27 (1995).
- [75] P. Schiavon, R. Birsa, K. Bos, F. Bradamante, A.S. Clough, S. Dalla Torre-Colautti, J.R. Hall, E. Heer, R. Hess, J.C. Kluyver, R.A. Kunne, C. Lechanoine-LeLuc, L. Linssen, A. Martin, Y. Onel, A. Penzo, D. Rapin, R.L. Shypit, F. Tassarotto, and A. Villari, Nucl. Phys. **A505**, 595 (1989).
- [76] R. Birsa, F. Bradamante, A. Bressan, S. Dalla Torre-Colautti, M. Giorgi, M. Lamanna, A. Martin, A. Penzo, P. Schiavon, F. Tassarotto, A.M. Zanetti, A. De Falco, M.P. Macciotta, A. Masoni, G. Puddu, S. Serici, A. Ahmidouch, E. Heer, R. Hess, C. Mascarini, D. Rapin, J. Arvieux, R. Bertini, J.C. Faivre, R.A. Kunne, and M. Agnello, Phys. Lett. B **339**, 325 (1994); Erratum-*ibid.* **405**, 389 (1997).
- [77] A. Bressan, R. Birsa, E. Bradamante, S. Dalla Torre-Colautti, M. Giorgi, M. Lamanna, A. Martin, P. Schiavon, F. Tassarotto, A.M. Zanetti, M.P. Macciotta, A. Masoni, G. Puddu, S. Serici, A. Ahmidouch, R. Heer, R. Hess, C. Lechanoine-Leluc, D. Rapin, J. Arvieux, R. Bertini, J.C. Faivre, R.A. Kunne, and M. Agnello, Nucl. Phys. **A625**, 10 (1997).
- [78] R. Birsa, F. Bradamante, S. Dalla Torre-Colautti, M. Giorgi, M. Lamanna, A. Martin, A. Penzo, P. Schiavon, F. Tassarotto, M.P. Macciotta, A. Masoni, G. Puddu, S. Serici, T. Niinikoski, A. Rijllart, A. Ahmidouch, E. Heer, R. Hess, R.A. Kunne, C. Lechanoine-LeLuc, C. Mascarini, D. Rapin, J. Arvieux, R. Bertini, H. Catz, J.C. Faivre, F. Perrot-Kunne, M. Agnello, F. Iazzi, B. Minetti, T. Bressani, E. Chiavassa, N. De Marco, A. Musso, and A. Piccotti, Phys. Lett. B **246**, 267 (1990).
- [79] R.A. Kunne, C.I. Beard, R. Birsa, K. Bos, F. Bradamante, D.V. Bugg, A.S. Clough, S. Dalla Torre-Colautti, J.A. Edgington, M. Giorgi, J.R. Hall, E. Heer, R. Hess, J.C. Kluyver, C. Lechanoine-LeLuc, L. Linssen, A. Martin, T.O. Niinikoski, Y. Onel, A. Penzo, D. Rapin, J.M. Rieubland, A. Rijllart, P. Schiavon, R.L. Shypit, F. Tassarotto, and A. Villari, Phys. Lett. B **261**, 191 (1991).
- [80] T. Ohsugi, M. Fujisaki, S. Kaneko, Y. Murata, K. Okamura, H. Kohno, M. Fukawa, R. Hamatsu, T. Hirose, S. Kitamura, T. Mamiya, T. Yamagata, T. Emura, I. Kita, and K. Takahashi, Il Nuovo Cimento **17A**, 456 (1973).

- [81] E. Eisenhandler, W.R. Gibson, C. Hojvat, P.I.P. Kalmus, L.C.Y. Lee, T.W. Pritchard, E.C. Usher, D.T. Williams, M. Harrison, W.H. Range, M.A.R. Kemp, A.D. Rush, J.N. Woulds, G.T.J. Arnison, A. Astbury, D.P. Jones, and A.S.L. Parsons, Nucl. Phys. **B113**, 1 (1976).
- [82] H. Kohno, S. Kaneko, Y. Murata, T. Ohsugi, K. Okamura, M. Fukawa, R. Hamatsu, T. Hirose, T. Mamiya, T. Yamagata, T. Emura, I. Kita, and K. Takahashi, Nucl. Phys. **B41**, 485 (1972).
- [83] R. Bertini, M. Costa, F. Perrot, H. Catz, A. Chaumeaux, J.Cl. Faivre, E. Vercellin, J. Arvieux, J. Yonnet, B. van den Brandt, J.A. Konter, D.R. Gill, S. Mango, G.D. Wait, E. Boschitz, W. Gyles, W. List, C. Otterman, R. Tacik, M. Wessler, E. Descroix, J.Y. Grossiord, and A. Guichard, Phys. Lett. B **228**, 531 (1989).
- [84] M. Kimura, M. Takanaka, R. Hamatsu, Y. Hattori, T. Hirose, S. Kitamura, T. Yamagata, T. Emura, I. Kita, K. Takahashi, H. Kohno, and S. Matsumoto, Il Nuovo Cimento **71A**, 438 (1982).
- [85] M. Bogdanski, T. Emura, S.N. Ganguli, A. Gurtu, S. Hamada, R. Hamatsu, E. Jeannet, I. Kita, S. Kitamura, J. Kishiro, H. Kohno, M. Komatsu, P.K. Malhotra, S. Matsumoto, U. Mehtani, L. Montanet, R. Raghavan, A. Subramanian, K. Takahashi, and T. Yamagata, Phys. Lett. **62B**, 117 (1976).
- [86] S. Banerjee, S.N. Ganguli, A. Gurtu, P.K. Malhorta, R. Raghavan, A. Subramanian, K. Sudhakar, M.M. Agarwal, J.M. Kohli, J.P. Lamba, I.S. Mittra, J.B. Singh, P.M. Sood, Dev Anand, P.V.K.S. Baba, G.L. Kaul, Y. Prakash, N.K. Rao, G. Singh, R. Hamatsu, T. Hirose, S. Kitamura, and T. Yamagata, Z. Phys. **C28**, 163 (1985).
- [87] M. Lamanna, A. Ahmidouch, R. Birsa, F. Bradamante, A. Bressan, T. Bressani, S. Dalla Torre-Colautti, M. Giorgi, E. Heer, R. Hess, R.A. Kunne, C. Lechanoine-Le Luc, A. Martin, C. Mascarini, A. Masoni, A. Penzo, D. Rapin, p. Schiavon, and E Tassarotto, Nucl. Phys. **B434**, 479 (1995).
- [88] R. Birsa, F. Bradamante, A. Bressan, S. Dalla Torre-Colautti, M. Giorgi, M. Lamanna, A. Martin, A. Penzo, P. Schiavon, F. Tassarotto, M.P. Macciotta, A. Masoni, G. Puddu, S. Serici, T. Niinikoski, A. Rijllart, A. Ahmidouch, E. Heer, R. Hess, C. Lechanoine-Leluc, C. Mascarini, D. Rapin, J.C. Faivre, F. Perrot-Kunne, J. Arvieux, R. Bertini, R.A. Kunne, F. Iazzi, B. Minetti, T. Bressani, E. Chiavassa, N. De Marco, A. Musso, and A. Piccotti, Phys. Lett. B **302**, 517 (1993).
- [89] A. Ahmidouch, R. Bertini, R. Birsa, F. Bradamante, A. Bressan, S. Dalla Torre-Colautti, M.

- Giorgi, E. Heer, R. Hess, F. Iazzi, M. Lamanna, C. Lechanoine-Leluc, A. Martin, G. Puddu, D. Rapin, R. Schiavon, and F. Tassarotto, Phys. Lett. B **380**, 235 (1996).
- [90] M.G. Albrow, S. Andersson/Almehed, B. Bošnjaković, C. Daum, F.C. Ern  , Y. Kimura, J.P. Lagnaux, J.C. Sens, and F. Udo, Nucl. Phys. **B37**, 349 (1972).
- [91] E. Leader, Phys. Lett. **60B**, 290 (1976).
- [92] R.A. Bryan, Phys. Rev. C **24**, 2659 (1981); *ibid.* **30**, 305 (1984); **39**, 783 (1989).
- [93] S. Klarsfeld, Phys. Lett. **126B**, 148 (1983).